NASA TN D-368

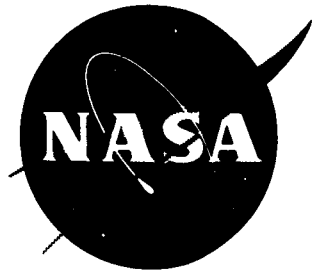

TECHNICAL NOTE
D-368

PRELIMINARY EXPERIMENTAL INVESTIGATION OF EFFECT OF FREE-STREAM TURBULENCE ON TURBULENT BOUNDARY-LAYER GROWTH

By S. J. Kline, A. V. Lisin, and B. A. Waitman

Stanford University

NATIONAL AERONAUTICS AND SPACE ADMINISTRATION

WASHINGTON

March 1960

NATIONAL AERONAUTICS AND SPACE ADMINISTRATION

TECHNICAL NOTE D-368

PRELIMINARY EXPERIMENTAL INVESTIGATION OF EFFECT OF FREE-STREAM TURBULENCE ON TURBULENT BOUNDARY-LAYER GROWTH

By S. J. Kline, A. V. Lisin, and B. A. Waitman

SUMMARY

The results of an experimental investigation of the effect of free-stream turbulence on the characteristics of the turbulent boundary layer on a flat plate are presented. With the exception of the final runs, the measurements available at the cessation of the work reported are of only moderately satisfactory accuracy. Despite this, the data presented are sufficient to demonstrate the following points.

The normally employed correlations for the turbulent boundary layer on a plate are, in effect, a limiting law for low turbulence in the free stream. Since the self-generated turbulence intensity in a turbulent boundary layer with low free-stream turbulence is of the order of 5 to 10 percent near the wall, this limiting law holds up to relatively high values of free-stream turbulence. However, when the free-stream turbulence is equal to or greater than the self-generated turbulence of the shear layer, considerable alterations in the boundary-layer characteristics occur. In particular, high values of free-stream turbulence increase the thickness of the boundary layer, create fuller velocity profiles, and raise the apparent value of wall shear. As would be expected, the distribution of intensity of velocity fluctuations through the boundary layer is also grossly altered. Such altered boundary layers do not conform to the "universal" velocity profiles in the form of the law of the wall or the law of the wake. A straight-line portion of the layer on a semilogarithmic plot still exists but its slope and location are altered and are shown to depend upon the imposed free-stream fluctuation intensity.

INTRODUCTION

The experimental work described herein was undertaken as a result of observations made by Moore and Kline in the diffuser work at Stanford University (refs. 1 and 2). Moore and Kline found that insertion of

rods upstream of the throat of a wide-angle diffuser affected the initiation of stall. Rods were found to retard and in some cases to prevent fully developed separation. The effectiveness of the rods in preventing separation was dependent on rod size.

Further study in a water channel indicated roughly that a threefold increase in boundary-layer thickness could be obtained merely by inserting $1\frac{1}{8}$-inch rods near the channel inlet. From the above observations it was decided that there may be an effect of turbulence in the free stream on turbulent boundary-layer growth.

Considerable work has been done on the effect of free-stream turbulence on boundary-layer transition and separation, for example, references 3, 4, and 5, and also on the effect of surface roughness on drag, heat-transfer coefficients, and boundary-layer thickness, for example, references 5, 6, and 7. Ludwieg and Tillman (ref. 8) reported a single test in which an increase in free-stream turbulence produced a 10-percent increase in friction coefficient. Wieghardt and Tillman (ref. 9) and Schubauer and Klebanoff (ref. 10) have noted that changes in free-stream turbulence affect the outer portion of the turbulent-boundary-layer profile. However, the search of the above references and others indicated that only meager, if any, data were available on the existence of the above-mentioned effect of free-stream turbulence on turbulent-boundary-layer growth, so it was concluded that a systematic experimental investigation of this effect should be undertaken.

The work reported here was conducted at Stanford University under the sponsorship and with the financial assistance of the National Advisory Committee for Aeronautics. This work included construction of a small variable-turbulence wind tunnel and completion of tests adequate to show that an important effect of free-stream turbulence on turbulent-boundary-layer growth does exist for high free-stream turbulence levels. It is suggested that further work should be done to provide the basis for correlation of this effect. Future measurements should include an investigation of the effects of positive and negative pressure gradients and should include careful measurements of wall shear stress.

NOMENCLATURE

Symbols

A,B	constants in logarithmic velocity profile, equation (2)

C_f wall shear coefficient, $\tau_o / \frac{1}{2} \rho \bar{U}_\infty^2$

D turbulence-promoter (rod) diameter, in.

f,g functions

I instantaneous current through hot-wire, ma

k equivalent uniform surface roughness

p static pressure, (lb force)/sq ft

q dynamic pressure, $\bar{U}^2 / 2g_c$, (lb force)/sq ft

Re Reynolds number, $\bar{U}x\rho/\mu$

U instantaneous velocity in x-direction, ft/sec

$\bar{U}^+ = \bar{U}/u^*$

u instantaneous velocity fluctuation about time average, in x-direction, $\bar{U}$ - U, ft/sec

u^* friction velocity, $\sqrt{\tau_o/\rho}$

x Cartesian coordinate measured parallel to tunnel axis from leading edge of plate, in.

y Cartesian coordinate measured normal to plate from plate surface, in.

$y^+ = (yu^*\rho)/\mu$

z Cartesian coordinate measured parallel to plate from plate center line, in.

δ boundary-layer thickness, in.

δ^* boundary-layer displacement thickness, in.

θ boundary-layer momentum thickness, in.

λ distance downstream of turbulence promoters, 9 + x, in.

μ	dynamic viscosity, (lb force)-sec/sq ft
ρ	fluid density, (lb mass)/cu ft
τ_o	wall shear stress, (lb force)/sq ft

Subscripts

b	boundary layer
ref	reference quantity
x	x-direction
1	station 1 (λ = 7.4 in.)
2	station 2 (λ = 18.6 in.; x = 9.6 in.)
3	station 3 (λ = 28.3 in.; x = 19.3 in.)
4	station 4 (λ = 47.6 in.; x = 38.6 in.)
∞	free stream

Notation

'	root-mean-square value
$(\bar{\ })$	time average value

EXPERIMENTAL APPARATUS

Wind Tunnel

The experimental work was conducted in a specially constructed variable-turbulence-intensity wind tunnel in the Mechanical Engineering Laboratory of Stanford University. The wind tunnel is of the open-return, suction type with a $5\frac{1}{2}$-inch-square test section (see fig. 1). The longitudinal component of turbulence intensity in the test section is variable from below 1 percent to above 20 percent. Various intensities are achieved by means of interchangeable screens or rods mounted near the beginning of the test section or just downstream of the damping section. The damping section has a flow area 2 feet square

and consists of nine 64-mesh, 4-mil wire diameter screens located every 2 inches. To prevent separation of the flow from the walls of the transition pieces and the consequent increase in turbulence intensity, the wall contour and rate of change of this contour were made continuous. The entrance section is made with elliptical walls while the contraction section has walls made up of cubic arcs (design data taken from Rouse and Hassan, ref. 11). The entrance section is mounted on wheels and track to make it movable for addition or change of screens in the damping section.

Immediately following the test section is a diffuser for the purpose of reducing the flow velocity in the long overhead duct leading from the test section to the blower. The blower is located about 30 feet from the test section to reduce the propagation of mechanical vibrations, flow pulsations, and noise from the blower to the test section.

Test Section

The test section of the wind tunnel is $5\frac{1}{2}$ inches square with a present maximum velocity of approximately 150 feet per second. The sides of the test section are made of Lucite (see fig. 2) to allow visual observations of the flow. Access taps in the top and sides provide for both horizontal and vertical traverses of the flow. The top taps are constructed to fit the micrometer traverse head described in the next section and shown in position in figure 2. The flat plate on which the boundary-layer measurements were made is located slightly below the center line of the test section and has its working surface facing up. The plate is made of brass and is finished on the working side with crocus cloth. The nose is faired to minimize downstream disturbances. Static-pressure taps of 0.020-inch diameter are located every 4 inches along the length of the plate.

The top of the test section is made of a perforated brass plate backed with a Fiberglas panel of varying porosity. The variation in porosity with length is such that a constant free-stream velocity and consequently a zero pressure gradient can be attained in the test section without making the passage divergent. A suction slot in the bottom of the test section, 4 inches downstream of the plate leading edge, allows adjustment of the location of the stagnation point on the nose of the plate.

Immediately ahead of the test section is the turbulence-promoting section. It is constructed so that any size rods up to those of 3/4-inch diameter may be inserted in a single row in either the horizontal, vertical, or crossed positions. In the present experiment the distance from the vertical rods to the plate leading edge was 9 inches.

Figure 3 shows 1/2-inch-diameter vertical rods inserted in the turbulence-promoting section.

Instrumentation

The hot-wire anemometer used in the present experimental work operates at a constant resistance for average velocity measurements but at constant current for turbulence-intensity measurements. For circuit description, theory, and operating instructions see reference 12.

Two wire sizes and materials were used for the hot-wire-anemometer filaments, 0.00035-inch-diameter tungsten and 0.000249-inch-diameter platinum. The initial work was done with a tungsten filament. However, as the work progressed, it was found that the filament calibration changed very rapidly and erratically. After a check of the circuit and components indicated no malfunction and since washing of the filament almost always brought the calibration back to its original line, it was concluded that the tungsten filaments are very susceptible to calibration changes due to bombardment by dirt particles carried in the airstream. Figure 4 shows a tungsten-filament calibration curve and the erratic shifts caused by dirt. A filter was mounted on the inlet to the tunnel and a calibration check was carried out before and after each run to prevent the inadvertent use of bad data. The platinum filaments were found to be more difficult to attach to the probe tips; however, once they were attached, the wire did not collect dirt as rapidly and hence far fewer erratic fluctuations in the calibration occurred (as seen in fig. 5).

The bridge circuit necessary for the measurement of average velocity and the amplifying and compensating circuits necessary for measurements of turbulence intensity were contained in the Model HWB hot-wire circuit manufactured by the Flow Corporation. A Tektronix type 512 cathode-ray oscilloscope was used to set the proper hot-wire compensation frequency as well as for visually observing the turbulent fluctuations. A Brown Electronik galvanometer was used in place of the galvanometer contained in the Flow Corporation circuit to provide added sensitivity and speed of reading. The voltmeter used in obtaining turbulence intensity was a Ballantine Laboratories Model 320 true root-mean-square voltmeter. The hot-wire probes were the two needle type probes made by Flow Corporation with an approximate distance of 1/8 inch between needle tips. The probes were modified slightly as described later in this section. A Foxboro micromanometer was used in obtaining the axial static pressure gradient. Conventional pitot-static probes, Kiel probes, and draft gages were used for measurements of free-stream velocity and for the hot-wire filament calibrations.

A creeper probe was designed and built for locating boundary-layer transition. The probe can be seen near the rear of the plate in figure 2. The probe is mounted on skids which ride on the plate. The impact tube on the nose of the heavy supporting rod is a 0.040-inch-diameter stainless steel tube flattened to a 0.01-inch height. With this probe velocities could be measured as close as 0.005 inch from the plate surface. The technique of locating boundary-layer transition with this probe is described in the following section. A specially made static-pressure probe was mounted on the creeper probe to check the validity of the static-pressure distribution measurements made with the taps drilled in the plate. The probe location was 5/8 inch above the plate and approximately on the vertical center plane of the test section.

A micrometer traverse head was used to position the hot-wire anemometer probes accurately in the y-direction. The device is such that the probe is clamped to the extension rod of a depth micrometer through a close-fitting ball bearing. The micrometer stock is rigidly fastened to the frame of the traverse head which in turn can be mounted on the wind tunnel. Thus, turning the micrometer would drive the probe up and down. The relative probe location could be determined to approximately 0.0002 inch by interpolation between the 0.001-inch calibrations on the micrometer. The backlash in the bearing was approximately 0.0002 inch. The micrometer head and probe can be seen mounted at station 3 in figure 2.

The vertical distance from the hot-wire-anemometer filament to the plate surface was determined by means of a thin, spring steel extension wire mounted on one of the filament-supporting needles of the hot-wire probe. The extension wire extended beyond the needle tip by 0.0019 inch. When a 0.00035-inch-diameter filament was soldered to the probe tips, the filament center line was about 0.0017 inch above the end of the extension wire. Thus, the distance of the filament from the plate would be known when the extension wire just touched the plate and closed an electric circuit. The point of closing of the circuit could be determined by a light and batteries in the circuit or by means of an ohmmeter. The latter method was more accurate since the probe could always be zeroed at the same value of resistance. This method was used to obtain the distance from the needle tips to the extension wire tip. The distance was measured several score times by three operators and in all cases was 0.0017 ± 0.0002 inch.

EXPERIMENTAL WORK

Check on Flow Conditions and Their Control

Prior to the taking of any experimental data, several short tests were made to see whether adequate control of the wind-tunnel variables

could be maintained. The following discussion presents some of the variables and how they were controlled.

Free-stream velocity profile.- Free-stream velocity profiles were obtained ahead of the plate (station 1) and at three locations along the plate (stations 2, 3, and 4) as a check on the tunnel flow symmetry and also on the secondary flows. Velocity traverses were made both horizontally and vertically ahead of the plate and horizontally at the three locations along the plate. The velocities were found to vary only slightly in the central 3-inch core of the flow, the greatest deviations from the average velocity occurring at the highest turbulence intensity. Several typical free-stream velocity profiles are shown in figure 6. The following table indicates the maximum deviations from the average free-stream velocity which were observed at any station for the given flow conditions.

Rod size, in.	Maximum deviation, percent, at station -			
	1	2	3	4
None	±0.4	±0.3	±0.2	±0.2
1/8	±2.2	±1.5	±1.4	±1.0
3/4	±3.2	±6.1	±4.3	±1.7

In all instances the velocity near the walls (outer region of the boundary layer) was higher than in the free stream. This effect is believed to be due to a secondary flow caused by suction through the top of the test section.

Axial static-pressure distribution.- The experimental data presented later in this section were obtained under the condition of a zero pressure gradient in the flow direction. The zero-pressure-gradient condition was achieved by means of suction through the porous upper wall of the tunnel (the wall opposite the plate) and by minor adjustment of the plate by means of its supporting screws. During the series of runs at 100 feet per second, the pressure was held constant to within ±0.7 percent of q_∞. During the runs of 50 feet per second, the pressure was held constant to within ±0.5 percent of q_∞. Typical pressure distributions are shown in figure 7. The pressure distribution was measured in two ways. The measurements were originally made by means of 0.020-inch-diameter static-pressure taps drilled in the plate and spaced axially at 4-inch intervals. These measurements were checked with a static-pressure probe mounted on the creeper probe described earlier. In this way measurements were taken at the plate surface and at 5/8 inch above the plate. The results agreed to well within the instrument sensitivity.

Location of boundary-layer transition.- In the present experimental work it was attempted to separate the direct effect of free-stream turbulence on the turbulent-boundary-layer growth from the variations in boundary-layer thickness due to a change in transition location with turbulence intensity. In the first series of runs (at 100 feet per second) the transition location was held to the first 3/4 inch of the plate for all turbulence intensities. To achieve a stable transition condition, the flow was made to approach the plate at a slight positive angle of attack. A stalled region just behind and above the nose of the plate resulted. The stall occupied a region 0.010 inch high by 3/8 inch long for all free-stream turbulence intensities and proved to be a very effective and stable transition initiator.

Transition was located by superposing measurements taken with a creeper probe on computed curves. From standard laminar and turbulent boundary-layer-profile equations, curves of $(q_\infty - q_b)/q_\infty$ versus x were plotted for constant y. The experimental points obtained with the creeper probe at an approximate distance of 0.005 inch from the plate indicated that transition always occurred within the first 3/4 inch of the plate (see fig. 8). The computed curves shown are the velocity heads at 0.005 inch from the plate.

In the second set of runs (at 50 feet per second) there was no angle of attack on the plate and a boundary-layer trip was used to initiate transition. The trip was a 0.009-inch-diameter wire located 3/8 inch downstream of the plate nose. The initiation of transition was determined as above and was always found to occur within the first 3 inches of the plate. As a point of interest, figure 9 shows the effect of free-stream turbulence and of the trip on transition location.

It should be noted that changes in the location of transition were very small and that the extent of the laminar and transition regions combined was less than 4 percent of the total length in all but two runs, where it did not exceed 7 percent. Consequently, the origin of the turbulent layer was assumed to be the leading edge of the plate in all cases. This should introduce no significant error in the data.

Control of free-stream turbulence intensity.- The range of axial free-stream turbulence intensities available in the variable-turbulence wind tunnel in which the present work was done was from 0.5 to 20 percent, the lower intensity being obtainable as a result of nine 0.004-inch-diameter, 64-mesh screens placed in the damping section of the wind tunnel (see fig. 1). The screens were a permanent part of the wind tunnel and acted as turbulence dampers and additionally flattened the velocity profiles. The ability of the screens to damp out upstream disturbances was checked by blocking one-half the flow just upstream of the screens. No change in the turbulence intensity or in the velocity profile in the test section could be perceived.

This result is not surprising since the screens were designed to produce a free-stream intensity of 0.05 percent. The discrepancy between this value and the 0.5 percent realized is due to the mechanical vibrations and pressure field arising from the only compressor available. Because of the added cost of a new compressor, it was decided to check the data for turbulence levels from 0.5 to 20 percent first, and to postpone the purchase of a quieter compressor until the need for it had definitely been established.

Turbulence intensities above 0.5 percent were obtained by inserting rods vertically just ahead of the test section. The leading edge of the plate on which the boundary-layer measurements were made was 9 inches downstream of the turbulence-promoting rods. Free-stream turbulence intensities were measured on the vertical centerline of the tunnel at stations located 7.4, 18.6, 28.3, and 47.6 inches downstream of the rods. The first station is ahead of the plate leading edge and the latter three locations are coincident with the stations where boundary-layer-profile measurements were made.

For initial turbulence intensities above the natural intensity of the tunnel (about 0.5 percent) the turbulence intensity decayed as the flow progressed downstream from the promoting rods. This decay caused a decrease in intensity along the plate for all initial turbulence intensities in excess of 0.5 percent. Figure 10 shows the effect of rod size D and distance from the rods λ on intensity. The experimental points are compared with a curve from Baines and Peterson (ref. 13) and appear to be reasonable although rather widely scattered.

Operating Procedures

Before any measurements were made in the wind tunnel, its flow characteristics and the control of variables were checked. The initial checks of free-stream velocity profiles, axial pressure gradient, boundary-layer transition stability, and free-stream turbulence-intensity control have been described in the preceding section. In addition to the initial checks the procedure below was followed to assure that flow conditions were constant and that the hot-wire-filament calibration had not changed:

(1) Wash hot-wire-anemometer filament in acid.

(2) Calibrate hot-wire anemometer against pitot-static probe over the range of velocities of interest.

(3) Establish flow conditions (free-stream velocity, pressure gradient, angle of attack).

(4) Check hot-wire-anemometer calibration in the free stream (at 100 feet per second).

(5) Zero hot-wire anemometer by means of extension wire and electric circuit.

(6) Make velocity traverse of boundary layer.

(7) Check hot-wire-filament calibration in free stream.

(8) Measure free-stream turbulence intensity.

(9) Remove hot-wire-anemometer probe from wind tunnel and wash filament.

(10) Repeat steps (4) through (9) at the other stations where boundary-layer-profile measurements are to be made.

(11) Measure free-stream turbulence at station 1.

(12) Run complete calibration of the hot-wire anemometer.

The calibration checks indicated any changes in the set free-stream velocity as well as in the filament calibration. If at any time the calibration checks or the final calibration did not agree with the initial calibration within 5 percent, the data obtained between the two calibrations were discarded. To make certain that the results of the hot-wire anemometer were correct, additional boundary-layer-profile measurements were made at stations 3 and 4 with a pitot-static probe covering the portion of the boundary layer which is accessible by this means.

To make certain that the changes in boundary-layer profile observed at 100 feet per second were due to changes in turbulence intensity and were not caused by wind-tunnel characteristics at that velocity or by the separated nose condition on the plate, additional data were taken with a platinum filament on the hot-wire anemometer at a velocity of 50 feet per second. The rigorous procedure of calibration checks was not necessary with the platinum filament as the calibrations were very stable.

Results of Effect of Free-Stream Turbulence on Boundary-Layer Growth

The primary data were taken at three locations on a flat plate with a free-stream velocity of 100 feet per second and at five turbulence

conditions. Turbulence-intensity measurements were made with a hot-wire-anemometer probe using a 0.00035-inch-diameter tungsten filament and operated at a constant current. Measurements of average velocity through the boundary layer were made with the same hot-wire probe operating at a constant resistance ratio.

The distance of the filament from the plate, dimension y, was determined by means of an electric circuit, a feeler wire, and a micrometer traverse head as described in the section on instrumentation. The range of initial longitudinal free-stream turbulence intensities under which the data were obtained was from 0.5 to 20 percent. The transition from laminar to turbulent boundary layer was fixed by means of the separated nose condition. The data obtained are presented in both dimensional and nondimensional forms in table 1. The results of the investigation are best seen in figure 11.

Figures 11(a), 11(b), and 11(c) show the boundary-layer profiles in dimensional form obtained for five free-stream turbulence conditions at stations 2, 3, and 4 (corresponding to length Reynolds numbers of 1/2, 1, and 2×10^6, respectively). The use of a nondimensional velocity and a dimensional distance makes it possible to eliminate the variable of free-stream velocity which was difficult to preset from run to run to closer than ±5 percent. The error in Reynolds number caused by using a velocity other than 100 feet per second is, of course, directly proportional to the error in the preset velocity. All of figures 11(a), 11(b), and 11(c) show the effect under investigation. However, because the boundary layer at stations 2 and 3 was quite thin, the effect of free-stream turbulence on the turbulent boundary layer can be seen best in figure 11(c) for station 4. Increased turbulence is seen to increase the boundary-layer thickness appreciably. In fact, a change in intensity from 0.5 to 20 percent at station 1 causes the boundary-layer thickness on the plate to increase approximately threefold. Between the edge of the boundary layer and the knee of the velocity curves the velocity profiles are seen to intersect so that the velocities near the knees of the profiles are higher at higher turbulence intensities. Both the increased thickness and increased velocity at the knee accompanying an increase in turbulence occur because of the more rapid interchange of energy between the free stream and the boundary layer at high turbulence intensities. As a result of the crossing of the curves there appears to be only a slight change with turbulence in both the boundary-layer displacement thickness δ^* and in momentum thickness θ. Both quantities have been computed for all the boundary-layer profiles by graphical integration. The scatter in the computed values was too large to allow construction of definitive curves of δ^* and θ versus x. However, there appeared to be a slight increase in both quantities with increased free-stream turbulence intensity. Values of δ^* and θ obtained by the graphical integration of the experimental boundary-layer

velocity profiles as well as those computed from a one-seventh-power velocity profile are tabulated in table 2.

Figures 11(d), 11(e), and 11(f) present the same data as those shown in figures 11(a), 11(b), and 11(c), but in nondimensional form. The boundary-layer thickness used to determine y/δ was found from the faired curve of $\bar{U}$ versus y. Note that δ is taken as the distance from the plate where the velocity is 99 percent of $\bar{U}_\infty$. The turbulence intensity at station 1 and the boundary-layer thickness are indicated on all the nondimensional profiles.

Early in the course of data taking it was observed that some of the measured boundary-layer profiles were quite erratic. Steps in velocity of up to nearly 15 feet per second were observed between adjacent points where velocity changes should have been small. It was found that over 50 percent of the boundary-layer profiles obtained contained some irregularity. A close check was made of all the succeeding hot-wire-anemometer calibrations, and it was found that the calibration curves were shifting appreciably. One such shift is shown in figure 4. The hot-wire-probe operating time between the two calibrations shown was approximately 1 hour. Shifts sometimes occurred gradually, sometimes in jumps of as much as 15 percent in velocity for a given current reading. When a check of the bridge circuit, of the probe, and of several filaments indicated no loose connections or faulty components, it was decided to check the hot-wire filament calibrations before, during, and after each run to make certain that no shifts in the calibration had occurred. Consequently, the early data were discarded, and the data described above were taken following the steps outlined under "Operating Procedures."

In order to check the results obtained with the hot-wire anemometer, data were taken at stations 3 and 4, with a pitot-static probe, at the same operating conditions as previously. The results are presented as before in table 3, and in figure 12. The same effect was observed in the later measurements as in the hot-wire measurements; however, it did not appear to be so great.

While the pitot-static data were being obtained, a further investigation of the hot-wire-anemometer calibration-shifting problem was made. It was eventually found that dirt in the airstream impinging on and sometimes sticking to the filament was the cause of the changes in calibration. A pair of impingement-type filters was placed in the wind tunnel just ahead of the damping screens to remove the larger dust particles. The frequency of the calibration shifts was reduced materially, but they were not eliminated. In the meantime a platinum hot-wire filament had been tried and was found to be far less susceptible to a dirty airstream even when dust was artificially added to the air. The

only problem encountered was the breaking of platinum filaments by large particles of dust and by careless handling.

To insure that the effect of turbulence on the boundary layer observed previously was not caused by wind-tunnel characteristics at the flow rate used or by the separated-nose condition, it was decided that data should be taken at a different flow rate and a nonstalled nose condition. Thus, boundary-layer profiles were obtained at a Reynolds number of 1×10^6 with a free-stream velocity of 50 feet per second. The data were taken with a platinum hot-wire-anemometer filament. The angle of attack on the nose of the plate was eliminated and boundary-layer transition was stabilized by means of a 0.009-inch-diameter trip wire placed on the plate surface, about 3/8 inch downstream of the leading edge. The effectiveness of the wire in stabilizing transition has been discussed previously. The data obtained are tabulated in table 4 and are presented in graphical form in figure 13.

The large change in boundary-layer thickness observed in the previous data was not apparent in the latter data. However, the velocity profiles of figure 13(a) show the same effects of turbulence on the velocity profile in the boundary layer. Figure 13(b) shows the experimental results in nondimensional form along with a one-seventh-power velocity profile. It was expected that one of the experimental velocity profiles obtained at a low-turbulence intensity would conform to the generally accepted one-seventh-power profile and that with increased turbulence the profiles would deviate from the one-seventh law. However, none of the profiles corresponds well to the one-seventh profile. This difficulty will be discussed in some detail later.

A summary of the boundary-layer thicknesses obtained at various turbulence intensities and values of x is shown in figure 14 for both the tungsten hot-wire-filament and the pitot-static-probe data. A computed curve, obtained from the relation

$$\delta/x = 0.376(\mathrm{Re})^{-0.2} \qquad (1)$$

is also shown for comparison. The faired curves were drawn using values of δ obtained by averaging the two sets of points. As discussed previously, high-turbulence intensities generate thicker boundary layers.

Measurements of Turbulence Intensity Within Boundary Layer

A number of measurements of longitudinal turbulence intensity were made through the boundary layer. They were made in the same way as the

free-stream turbulence measurements with distance from the plate determined as in the velocity profile measurements. Several turbulence-intensity distributions are shown in figure 15. Measurements were made with a hot-wire filament at length Reynolds numbers of 1×10^6 and 2×10^6 with 3/4-inch-diameter turbulence-promoting rods in the wind tunnel. The intensity distribution is seen to be quite independent of the length Reynolds number for a given free-stream turbulence condition. Furthermore, the data for low free-stream turbulence intensity check the comparable measurements of Klebanoff (ref. 14) quite well, but the intensity distribution for high free-stream turbulence is greatly different.

Further Results With Modified Wind Tunnel

Since the results reported above were not entirely satisfactory in the sense that the values of displacement and momentum thickness of the boundary layer scatter unduly and the velocity profiles at the lower values of turbulence level exhibit some unexplained intersections, a further check was instituted by comparing the results obtained for mean velocity profile with standard correlations. It was found that the velocity profile form did not check the standard forms given, for example, by Clauser (ref. 15). Furthermore, the value of boundary-layer thickness found for the low-turbulence runs lies approximately 15 to 20 percent below the usually accepted value given by equation (1) as shown in figure 14.

These anomalous results raise some question regarding the validity of the data and, accordingly, a further study was instituted. After investigating various matters it was found that a secondary flow in the boundary layers of the side walls and on the plate was occurring because of the effect of suction through the top panel. The effect of the suction on the main flow was very small and had been overlooked in the checks of flow conditions; however, the effect on the boundary layer was considerable. Therefore, in order to check the validity of the data taken previously, additional runs were made with the suction panel of the wind tunnel blocked. The test plate was tilted slightly to achieve zero pressure gradient again. The results of these tests confirm the prior findings and also probably explain the discrepancies observed in the earlier results.

The procedures employed in this last set of tests were the same as those described previously; however, only traverses with pitot probes were made. Plots of the observed velocity profiles are compared with the accepted correlations of Schultz-Grunow (ref. 16) in figure 16 and the comparison for the low free-stream turbulence conditions is given in figure 16(a). The values of C_f used in forming u^* were obtained

from replots of the velocity profiles using the method suggested by Clauser (ref. 15). The good agreement with standard form is evident.

With standard profiles established for low free-stream turbulence, the variations with intensity, as found previously, were checked. Results are shown in figure 17. Figure 17(a) shows an increase of approximately 50 percent in the 99-percent boundary-layer thickness with increased free-stream turbulence. It also suggests a moderate increase in the value of wall shear with increased free-stream turbulence. Figure 17 also shows substantial increases in δ^* and θ. In short, the results as found previously with nonstandard velocity profiles are substantiated by the effects shown with "standard type" profiles.

Use of the standard profiles, however, leads to further conclusions. When the velocity profiles are standard, the effects of free-stream intensity variations at small values are not as great as with nonstandard types. This definitely suggests that the small irregular variations in velocity profile at the lower free-stream intensities in the early data are probably due to variation in suction rather than to free-stream conditions. The effect of suction also explains the fact that δ is lower than the standard value in figure 14 for the lower intensity cases. As shown in figure 16(b) for $Re = 2 \times 10^6$, up to a free-stream longitudinal turbulence intensity of approximately 4 percent at the nose of the plate, fairly small changes in profile with intensity are found. These layers therefore will correlate in the usual forms of the law of the wall and the law of the turbulent wake. Therefore it can be concluded that these layers are essentially wall-dominated layers.

However, when the free stream has a large turbulence intensity the boundary layer is no longer wall dominated and its character is altered considerably; it no longer satisfies the law of the wall and the law of the wake. This is clearly shown by the lowest set of data points in figure 16(b).

The alteration in the character of the boundary layer, as evidenced by the distortion of the velocity profile, leads to two questions: (1) Does the velocity profile of a turbulent boundary layer with a very high free-stream intensity agree with the usual "universal correlation"? (2) If the velocity profiles with a high free-stream intensity will not conform to the universal correlation, can they still be represented at least by a straight line on a semilogarithmic plot?

In order to check whether the velocity profile at high free-stream intensity will agree with standard form, the profiles were plotted according to the method suggested by Clauser (ref. 15) and the indicated value of u^* taken from the curves. This value was then used

to normalize the velocity profiles as shown in figure 16(b). These profiles are of the form

$$\overline{U}^{+} = \frac{\overline{U}}{u^*} = A \log_e y^{+} + B \tag{2}$$

It is clearly evident that, while the curves at the low free-stream intensities up to 4 percent fall back on the accepted curve, the dimensionless profile for the high free-stream intensity is no longer in agreement with the usual result. This shift of the curve is an uncorrelated effect of free-stream turbulence intensity. Therefore, for very high values of free-stream turbulence, which produce layers which are not wall dominated, the velocity profiles cannot be resolved to the standard universal correlation of the semilogarithmic nature. This agrees with the large shift in intensity profile shown in figure 15. It also implies a shift in the value of C_f from the standard values at high turbulence levels; it must thus follow that the skin-friction law for high external turbulence is not known.

Regarding the question of whether the nondimensional profile will have a straight portion on a semilogarithmic plot, figure 16(b) suggests that it does. However, no firm conclusion can be reached on this point without further information. In the original argument as proposed by Millikan (ref. 17) such straight-line behavior on a semilogarithmic plot was based on the fact that there was complete similarity of boundary-layer profiles in the direction of flow. This implies a similarity of conditions in the free stream also independent of flow direction, a condition that is not fulfilled in the present tests where free-stream turbulence of necessity decays in the direction of flow.

In Millikan's original argument he bases the derivation of the straight-line portion of the boundary layer on the fact that both of the expressions

$$\overline{U}^{+} = f\left(\frac{\rho y u^*}{\mu}, \frac{y}{k}\right) \quad \text{where} \quad (y \to 0) \tag{3}$$

and

$$\frac{\overline{U}_\infty - \overline{U}}{u^*} = g\left(\frac{y}{\delta}\right) \quad \text{where} \quad \left(\frac{y}{\delta}\right) \to 0 \tag{4}$$

are known to apply. However, for the present conditions this is not known to be the case and would constitute an unwarranted assumption based on the data available. Hence no firm conclusion can be reached

on the second question. Despite this, the data of figure 16(b) suggest that the second question can probably be answered in the affirmative.

Stanford University,
Stanford, Calif., May 15, 1958.

REFERENCES

1. Moore, C. A., and Kline, S. J.: Investigation of Airfoils, Plates, Grids, and Rods for Boundary Layer Control in Subsonic Diffusers. Contract NAw-6317, NACA and Stanford Univ., Aug. 16, 1954.

2. Moore, C. A., and Kline, S. J.: Some Effects of Vanes and of Turbulence on Two-Dimensional Wide-Angle Subsonic Diffusers. NACA TN 4080, 1958.

3. Dryden, H. L., Schubauer, G. B., Mock, W. C., Jr., and Skramstad, H. K.: Measurements of Intensity and Scale of Wind-Tunnel Turbulence and Their Relation to the Critical Reynolds Number of Spheres. NACA Rep. 581, 1937.

4. Liepmann, H. W., and Fila, G. H.: Investigations of Effects of Surface Temperature and Single Roughness Elements on Boundary-Layer Transition. NACA Rep. 890, 1947. (Supersedes NACA TN 1196.)

5. Geidt, W. H.: Effect of Turbulence Level of Incident Air Stream on Local Heat Transfer Coefficient and Skin Friction on a Cylinder. Jour. Aero. Sci., vol. 18, no. 11, Nov. 1951, p. 725.

6. Gelder, T. F., and Lewis, J. P.: Comparison of Heat Transfer From an Airfoil in Natural and Simulated Icing Conditions. NACA TN 2480, 1951.

7. Klebanoff, P. S., and Diehl, Z. W.: Some Features of Artificially Thickened Fully Developed Turbulent Boundary Layers with Zero Pressure Gradient. NACA Rep. 1110, 1952. (Supersedes NACA TN 2475.)

8. Ludwieg, H., and Tillman, W.: Investigation of Wall Shearing Stress in Turbulent Boundary Layers. NACA TN 1384, 1947.

9. Wieghardt, K., and Tillman, W.: On the Turbulent Friction Layer for Rising Pressure. NACA TM 1314, 1951.

10. Schubauer, G. B., and Klebanoff, P. S.: Investigation of Separation of Turbulent Boundary Layer. NACA Rep. 1030, 1951. (Supersedes NACA TN 2133.)

11. Rouse, H., and Hassan, M. M.: Cavitation Free Inlets and Contractions. Mech. Eng., vol. 71, no. 3, Mar. 1949, pp. 213-216.

12. Anon.: Model HWB Hot Wire Anemometer Theory and Instructions. Flow Corp. (Cambridge, Mass.), 1955.

13. Baines, W. D., and Peterson, E. G.: An Investigation of Flow Through Screens. Trans. ASME, vol. 73, no. 5, July 1951, p. 467.

14. Klebanoff, P. S.: Characteristics of Turbulence in a Boundary Layer with Zero Pressure Gradient. NACA Rep. 1247, 1955. (Supersedes NACA TN 3178.)

15. Clauser, F. H.: Turbulent Boundary Layers in Adverse Pressure Gradient. Jour. Aero. Sci., vol. 21, no. 2, Feb. 1954, pp. 91-108.

16. Schultz-Grunow, F.: New Frictional Resistance Law for Smooth Plates. NACA TM 986, 1941.

17. Millikan, Clark B.: A Critical Discussion of Turbulent Flows in Channels and Circular Tubes. Proc. Fifth Int. Cong. Appl. Mech. (Sept. 1938, Cambridge, Mass.), John Wiley & Sons, Inc., 1939, pp. 386-392.

TABLE 1.- BOUNDARY-LAYER VELOCITY PROFILE DATA TAKEN WITH TUNGSTEN HOT-WIRE-ANEMOMETER PROBE FOR RUNS OF 100 FEET PER SECOND

(a) No rod

Station 2 ($Re = 0.5 \times 10^6$)				Station 3 ($Re = 1 \times 10^6$)				Station 4 ($Re = 2 \times 10^6$)			
y	y/δ	$\bar{U}$	$\bar{U}/\bar{U}_\infty$	y	y/δ	$\bar{U}$	$\bar{U}/\bar{U}_\infty$	y	y/δ	$\bar{U}$	$\bar{U}/\bar{U}_\infty$
0.0016	0.007	55.1	0.553	0.0017	0.004	50.2	0.472	0.0017	0.003	29.0	0.285
.0026	.012	60.8	.610	.0029	.008	57.1	.536	.0026	.004	35.3	.348
.0036	.017	62.5	.627	.0039	.010	59.9	.561	.0036	.005	42.5	.419
.0046	.022	64.7	.649	.0049	.013	61.2	.577	.0046	.007	46.4	.456
.0056	.026	66.1	.663	.0059	.015	63.5	.596	.0056	.009	50.3	.495
.0076	.036	69.0	.692	.0079	.021	66.1	.620	.0076	.012	53.3	.526
.0096	.045	70.0	.702	.0099	.026	67.7	.633	.0096	.015	55.4	.545
.0126	.060	71.2	.714	.0129	.034	69.2	.650	.0116	.018	58.4	.575
.0156	.074	73.0	.732	.0179	.047	70.9	.664	.0156	.024	60.4	.595
.0206	.098	73.3	.735	.0229	.060	71.9	.674	.0206	.032	61.1	.601
.0253	.121	75.2	.754	.0329	.086	73.0	.685	.0256	.039	63.1	.621
.0306	.146	77.9	.781	.0429	.112	76.1	.713	.0356	.054	63.9	.629
.0406	.194	78.3	.785	.0629	.165	80.4	.754	.0556	.087	67.0	.660
.0506	.242	81.9	.821	.0829	.217	82.8	.776	.0856	.132	70.0	.689
.0606	.290	82.7	.829	.1129	.296	84.8	.795	.1356	.209	74.8	.737
.0706	.338	84.8	.850	.1429	.375	90.3	.849	.1856	.286	78.3	.771
.0906	.434	88.8	.890	.1729	.454	93.2	.876	.2356	.362	82.8	.814
.1106	.529	91.7	.919	.2229	.585	98.2	.921	.2856	.440	85.7	.841
.1406	.672	95.0	.952	.2729	.717	101.8	.950	.3356	.516	89.9	.885
.1706	.816	97.2	.974	.3229	.848	104.2	.974	.3856	.594	91.8	.902
.2206	1.055	99.8	1.000	.3729	.979	106.1	.983	.4356	.671	93.2	.919
.2706		99.3	.995	.4229	1.110	106.5	1.000	.4856	.749	97.0	.953
.3206		99.3	.995	.4729		106.5	1.000	.5356	.825	97.8	.961
.3706		100.1	1.003	.5229		106.5	1.000	.5856	.902	99.0	.974
.4706		99.3	.995	.6229		106.5	1.000	.6356	.979	100.0	.986
.6706		99.8	1.000					.6856	1.055	101.3	.992
.8706		99.8	1.000					.7356		101.5	1.000
								.7856		101.5	1.000
								.8856		101.5	1.000
								.9856		101.5	1.000

TABLE 1.- BOUNDARY-LAYER VELOCITY PROFILE DATA TAKEN WITH TUNGSTEN HOT-WIRE-ANEMOMETER PROBE FOR RUNS OF 100 FEET PER SECOND - Continued

(b) 1/8-inch-diameter rod

Station 3 ($Re = 1 \times 10^6$)				Station 4 ($Re = 2 \times 10^6$)			
y	y/δ	$\bar{U}$	$\bar{U}/\bar{U}_\infty$	y	y/δ	$\bar{U}$	$\bar{U}/\bar{U}_\infty$
0.0017	0.004	50.1	0.502	0.0017	0.003	43.6	0.428
.0024	.006	53.9	.540	.0031	.005	52.5	.515
.0034	.009	58.8	.589	.0051	.008	56.7	.556
.0044	.012	60.2	.603	.0081	.013	62.8	.616
.0054	.014	62.0	.621	.0111	.018	65.8	.645
.0064	.017	63.1	.632	.0141	.023	66.9	.655
.0084	.022	65.5	.656	.0241	.039	69.3	.680
.0114	.030	68.0	.681	.0341	.056	71.9	.705
.0164	.043	70.5	.706	.0541	.089	73.9	.724
.0214	.056	72.4	.725	.1041	.171	79.7	.781
.0264	.070	73.2	.733	.1541	.253	85.7	.840
.0364	.096	75.4	.756	.2041	.334	87.2	.856
.0564	.149	79.2	.794	.2541	.417	89.2	.876
.0764	.201	79.9	.811	.3041	.499	92.7	.909
.0964	.255	84.8	.850	.3541	.581	93.1	.913
.1164	.308	86.9	.871	.4041	.662	96.1	.942
.1464	.387	91.1	.913	.4541	.743	98.3	.964
.1764	.466	92.3	.925	.5041	.826	98.0	.959
.2164	.571	93.6	.938	.5541	.908	100.0	.981
.2664	.704	97.9	.981	.6041	.990	102.0	.998
.3164	.836	97.9	.981	.6541	1.071	100.5	.981
.3664	.969	98.8	.990	.7041		102.3	1.002
.4164	1.102	98.8	.990	.7541		102.0	.998
.4664		99.2	.994	.8041		102.3	1.002
.5164		100.4	1.006	.9041		102.0	.998
.5664		99.2	.994				
.6164		99.2	.994				
.6664		100.4	1.006				

TABLE 1.- BOUNDARY-LAYER VELOCITY PROFILE DATA TAKEN WITH TUNGSTEN HOT-WIRE-ANEMOMETER PROBE FOR RUNS OF 100 FEET PER SECOND - Continued

(c) 3/8-inch-diameter rod

Station 2 ($Re = 0.5 \times 10^6$)				Station 3 ($Re = 1 \times 10^6$)				Station 4 ($Re = 2 \times 10^6$)			
y	y/δ	$\bar{U}$	$\bar{U}/\bar{U}_\infty$	y	y/δ	$\bar{U}$	$\bar{U}/\bar{U}_\infty$	y	y/δ	$\bar{U}$	$\bar{U}/\bar{U}_\infty$
0.0017	0.007	58.1	0.574	0.0017	0.003	51.1	0.472	0.0017	0.002	45.6	0.454
.0028	.011	63.9	.632	.0022	.003	56.4	.521	.0037	.005	56.1	.557
.0038	.015	64.9	.642	.0032	.005	59.9	.552	.0067	.009	60.8	.606
.0048	.019	67.2	.666	.0042	.006	62.2	.575	.0097	.013	61.2	.610
.0058	.023	68.1	.674	.0052	.008	63.7	.588	.0147	.020	68.0	.677
.0078	.031	72.5	.718	.0062	.009	65.1	.601	.0197	.027	69.5	.692
.0098	.039	72.5	.718	.0072	.011	66.8	.617	.0297	.040	70.6	.702
.0118	.048	74.2	.736	.0092	.014	68.9	.637	.0397	.054	73.7	.732
.0138	.056	75.3	.747	.0112	.017	68.9	.637	.0547	.074	74.8	.744
.0188	.076	77.0	.762	.0132	.020	70.9	.654	.0747	.101	79.3	.789
.0238	.096	79.2	.785	.0172	.026	71.7	.661	.0997	.135	79.7	.793
.0288	.116	80.9	.801	.0222	.032	73.8	.681	.1247	.168	82.1	.816
.0388	.136	83.0	.821	.0272	.041	74.7	.689	.1747	.236	85.0	.845
.0438	.176	83.0	.821	.0372	.056	75.3	.695	.2247	.304	89.3	.890
.0538	.217	83.7	.828	.0472	.071	80.0	.739	.2747	.371	91.9	.915
.0838	.338	89.4	.885	.0572	.086	81.1	.749	.3247	.439	92.8	.922
.1338	.540	91.5	.906	.0772	.116	85.7	.790	.3747	.506	92.8	.922
.1838	.740	95.3	.943	.0972	.146	87.1	.805	.4247	.574	94.1	.936
.2338	.943	101.2	1.002	.1172	.176	88.2	.816	.4747	.641	97.4	.969
.2838	1.143	103.6	1.023	.1372	.206	90.5	.836	.5247	.709	95.7	.952
.3338		99.6	.986	.1672	.251	91.4	.844	.5742	.776	97.4	.969
.3838		102.2	1.011	.1972	.296	92.8	.854	.6247	.844	102.2	1.017
.4338		100.1	.991	.2372	.356	93.9	.867	.6747	.911	98.7	.982
.4838		98.8	.978	.2872	.431	97.8	.902	.7247	.979	98.7	.982
.5838		98.8	.978	.3372	.506	97.8	.902	.7747	1.046	100.5	1.000
.6838		98.8	.978	.3872	.581	97.8	.902	.8247		100.5	1.000
				.4872	.733	102.7	.943	.9247		100.5	1.000
				.5872	.883	105.3	.968	1.0247		100.5	1.000
				.6372	.959	107.0	.984				
				.6872	1.033	108.2	1.000				
				.7372		108.2	1.000				
				.7872		108.2	1.000				
				.8372		108.2	1.000				
				.9372		108.2	1.000				

TABLE 1.- BOUNDARY-LAYER VELOCITY PROFILE DATA TAKEN WITH TUNGSTEN HOT-WIRE-ANEMOMETER PROBE FOR RUNS OF 100 FEET PER SECOND - Continued

(d) 1/2-inch-diameter rod

Station 2 ($Re = 0.5 \times 10^6$)				Station 3 ($Re = 1 \times 10^6$)				Station 4 ($Re = 2 \times 10^6$)			
y	y/δ	$\bar{U}$	$\bar{U}/\bar{U}_\infty$	y	y/δ	$\bar{U}$	$\bar{U}/\bar{U}_\infty$	y	y/δ	$\bar{U}$	$\bar{U}/\bar{U}_\infty$
0.0017	0.006	52.4	0.524	0.0017	0.004	48.0	0.480	0.0017	0.001	43.1	0.422
.0022	.007	55.5	.555	.0024	.006	55.3	.553	.0027	.002	53.5	.524
.0032	.011	59.3	.593	.0034	.009	61.6	.616	.0037	.003	55.2	.551
.0042	.014	65.8	.658	.0044	.012	63.7	.637	.0047	.004	57.7	.566
.0052	.017	66.1	.661	.0064	.017	67.3	.673	.0057	.005	60.6	.594
.0062	.021	69.0	.690	.0084	.022	69.4	.694	.0077	.007	63.5	.624
.0072	.024	71.2	.712	.0104	.027	71.2	.712	.0097	.008	64.4	.630
.0092	.030	72.4	.724	.0134	.035	73.2	.732	.0127	.011	67.3	.650
.0122	.040	75.4	.754	.0184	.048	75.5	.755	.0177	.015	70.2	.687
.0172	.057	79.2	.792	.0234	.062	76.5	.765	.0277	.023	73.1	.717
.0227	.074	80.5	.805	.0284	.075	79.6	.796	.0377	.032	73.8	.724
.0272	.090	81.2	.812	.0334	.088	80.5	.805	.0577	.048	76.5	.750
.0372	.123	85.1	.851	.0434	.114	80.9	.809	.0777	.065	78.9	.772
.0422	.139	86.4	.864	.0534	.140	82.5	.825	.1077	.091	79.2	.776
.0622	.205	87.2	.872	.0634	.167	84.5	.845	.1377	.116	82.4	.807
.0822	.271	88.9	.889	.0834	.219	87.8	.878	.1777	.149	84.2	.826
.1122	.371	92.7	.927	.1034	.272	88.5	.885	.2277	.191	88.1	.863
.1521	.503	92.7	.927	.1234	.325	90.6	.906	.2777	.233	89.1	.874
.2022	.667	97.4	.974	.1434	.378	94.0	.940	.3277	.275	92.5	.906
.2522	.832	100.2	1.002	.1634	.430	95.5	.955	.3777	.317	93.4	.915
.3022	.998	98.2	.982	.2134	.561	96.5	.965	.4277	.360	94.0	.920
.3522	1.162	99.4	.994	.2634	.694	96.5	.965	.5277	.444	97.7	.957
.4022		100.0	1.000	.3134	.825	98.5	.985	.6277	.528	98.1	.963
.4522		100.0	1.000	.3634	.957	100.0	1.000	.7277	.611	98.1	.963
.5022		99.4	.994	.4134	1.082	99.0	.990	.8277	.696	98.1	.963
.6022		100.0	1.000	.4634		97.9	.979	.9277	.780	100.0	.980
.8022		100.2	1.002	.5134		100.0	1.000	1.0277	.864	100.0	.980
1.0022		100.0	1.000	.5634		100.0	1.000	1.1277	.948	105.0	1.004
				.6634		100.0	1.000	1.2277	1.031	105.0	1.004
				.9634		98.5	.985	1.3277		103.6	.997

TABLE 1.- BOUNDARY-LAYER VELOCITY PROFILE DATA TAKEN WITH TUNGSTEN HOT-WIRE-ANEMOMETER PROBE FOR RUNS OF 100 FEET PER SECOND - Concluded

(e) 3/4-inch-diameter rod

Station 2 ($Re = 0.5 \times 10^6$)				Station 3 ($Re = 1 \times 10^6$)				Station 4 ($Re = 2 \times 10^6$)			
y	y/δ	$\bar{U}$	$\bar{U}/\bar{U}_\infty$	y	y/δ	$\bar{U}$	$\bar{U}/\bar{U}_\infty$	y	y/δ	$\bar{U}$	$\bar{U}/\bar{U}_\infty$
0.0017	0.004	53.9	0.537	0.0016	0.002	49.1	0.475	0.0017	0.001	42.6	0.418
.0021	.005	56.1	.560	.0024	.003	53.9	.520	.0020	.001	45.3	.444
.0031	.008	62.7	.624	.0034	.004	59.2	.571	.0030	.002	49.5	.485
.0041	.011	67.7	.675	.0044	.005	62.0	.598	.0040	.003	52.0	.510
.0061	.016	71.1	.708	.0054	.007	67.3	.649	.0060	.004	58.1	.570
.0081	.021	74.5	.741	.0064	.008	68.3	.660	.0080	.005	60.1	.589
.0101	.027	76.8	.764	.0084	.010	69.8	.674	.0100	.006	62.7	.614
.0121	.032	77.8	.774	.0124	.015	72.9	.702	.0130	.008	63.7	.624
.0161	.042	78.0	.776	.0164	.020	75.6	.727	.0180	.012	64.9	.637
.0201	.053	79.0	.786	.0204	.025	77.0	.743	.0280	.018	68.1	.668
.0281	.074	82.2	.808	.0304	.037	80.1	.772	.0380	.025	69.9	.686
.0381	.100	84.1	.838	.0404	.049	82.9	.799	.0580	.038	72.5	.711
.0481	.127	86.7	.864	.0604	.073	85.3	.823	.0780	.051	76.0	.744
.0681	.179	89.5	.891	.0804	.097	87.0	.838	.1280	.084	81.1	.794
.0881	.232	90.2	.898	.1004	.122	89.1	.859	.1780	.116	83.1	.816
.1181	.311	92.2	.918	.1304	.158	93.3	.899	.2280	.149	86.7	.849
.1481	.390	92.2	.918	.1804	.218	95.1	.916	.3280	.214	89.9	.880
.1881	.495	93.8	.934	.2304	.279	96.2	.927	.4280	.280	91.1	.892
.2381	.627	95.7	.953	.2804	.340	98.2	.949	.5280	.345	94.3	.925
.2881	.759	96.1	.957	.3304	.400	98.2	.949	.6280	.410	95.0	.930
.3381	.890	98.6	.932	.3804	.461	99.2	.957	.7280	.475	97.9	.959
.3881	1.022	100.2	.999	.4304	.522	101.6	.979	.8280	.541	97.9	.959
.4381		100.2	.999	.4804	.582	103.0	.991	.9280	.606	100.5	.985
.4881		99.8	.994	.5304	.642	101.4	.975	1.0280	.672	98.4	.964
.5381		100.2	.999	.5804	.704	101.6	.978	1.1280	.736	98.4	.964
.7381		100.5	1.001	.6304	.764	102.5	.986	1.2280	.803	99.2	.972
.9381		100.5	1.001	.6304	.825	102.2	.983	1.3280	.869	100.5	.985
1.0381		100.3	1.000	.7304	.885	102.2	.983	1.4280	.934	100.5	.985
				.8304	1.007	103.2	.995	1.5280	.998	102.2	1.002
				.9304		102.8	.992	1.6280	1.063	102.4	1.004
				1.0304		103.6	1.000	1.7280		101.4	.994
				1.1304		103.6	1.000	2.0280		102.4	1.004

TABLE 2.- MEASURED AND COMPUTED VALUES OF δ, δ^*, and θ FOR VARIOUS REYNOLDS NUMBERS AND TURBULENCE-PROMOTING-ROD SIZES

Re_x	Quantity	Measuring device	Measured value for rod diam. of -					Computed value
			None	1/8 in.	3/8 in.	1/2 in.	3/4 in.	
0.5×10^6	δ	Tungsten hot-wire	0.21	-----	0.24	0.30	0.38	0.23
	δ^*	Tungsten hot-wire	.025	-----	.026	.025	.031	.025
	θ	Tungsten hot-wire	.020	-----	.022	.022	.027	.023
1	δ	Tungsten hot-wire	.38	0.39	.66	.38	.82	.46
	δ	Pitot-static probe	.35	.44	.61	.56	.59	
	δ^*	Tungsten hot-wire	.052	.040	.079	.026	.053	.057
	δ^*	Pitot-static probe	.058	.057	.058	.051	.050	
	θ	Tungsten hot-wire	.041	.033	.075	.022	.045	.045
	θ	Pitot-static probe	.035	.042	.046	.047	.038	
2	δ	Tungsten hot-wire	.65	.61	.74	1.10	1.52	.80
	δ	Pitot-static probe	.65	.75	.95	.89	.88	
	δ^*	Tungsten hot-wire	.103	.075	.075	.100	.130	.100
	δ^*	Pitot-static probe	.098	.117	.100	.093	.083	
	θ	Tungsten hot-wire	.077	.059	.061	.083	.100	.078
	θ	Pitot-static probe	.075	.087	.079	.074	.066	

TABLE 3.- BOUNDARY-LAYER VELOCITY PROFILE DATA TAKEN WITH PITOT-STATIC PROBE FOR RUNS OF 100 FEET PER SECOND

(a) No Rod

Station 3 ($Re = 1 \times 10^6$)				Station 4 ($Re = 2 \times 10^6$)			
y	y/δ	$\bar{U}$	$\bar{U}/\bar{U}_\infty$	y	y/δ	$\bar{U}$	$\bar{U}/\bar{U}_\infty$
0.014	0.040	61.3	0.618	0.014	0.021	58.1	0.590
.015	.043	61.4	.619	.015	.023	57.6	.585
.017	.049	62.5	.630	.017	.026	59.1	.600
.020	.057	63.5	.640	.019	.029	59.6	.605
.022	.063	64.4	.649	.022	.034	60.5	.614
.024	.069	64.9	.654	.024	.037	61.0	.619
.026	.074	65.5	.660	.027	.041	62.0	.630
.028	.080	66.0	.665	.029	.045	62.4	.634
.030	.086	66.4	.669	.032	.049	62.9	.639
.033	.094	67.1	.676	.034	.052	63.1	.641
.035	.100	67.6	.681	.037	.057	63.6	.646
.038	.108	68.2	.687	.042	.065	64.5	.655
.040	.114	68.6	.691	.047	.072	65.1	.661
.045	.128	69.6	.701	.052	.080	66.0	.670
.050	.143	70.6	.711	.057	.088	66.5	.675
.055	.157	71.5	.720	.062	.095	67.0	.681
.060	.171	72.1	.726	.072	.111	68.3	.694
.064	.183	73.1	.736	.092	.141	70.1	.722
.070	.200	73.9	.745	.112	.172	72.0	.731
.090	.257	76.6	.772	.162	.249	75.7	.781
.110	.314	79.3	.799	.212	.326	79.3	.805
.160	.457	84.9	.855	.312	.480	85.1	.865
.210	.600	89.6	.903	.412	.634	90.1	.915
.310	.886	96.9	.976	.512	.788	94.2	.957
.410	1.171	99.0	.998	.612	.942	97.0	.985
.510	1.459	99.3	1.000	.712	1.095	98.1	.996
.610	1.742	99.3	1.000	.812	1.248	98.5	1.000
.710	2.028	99.3	1.000	.912	1.401	98.5	1.000
				1.012	1.558	98.4	.999

TABLE 3.- BOUNDARY-LAYER VELOCITY PROFILE DATA TAKEN WITH PITOT-STATIC PROBE FOR RUNS OF 100 FEET PER SECOND - Continued

(b) 1/8-inch-diameter rod

Station 3 ($Re = 1 \times 10^6$)				Station 4 ($Re = 2 \times 10^6$)			
y	y/δ	$\bar{U}$	$\bar{U}/\bar{U}_\infty$	y	y/δ	$\bar{U}$	$\bar{U}/\bar{U}_\infty$
0.014	0.032	64.3	0.639	0.014	0.019	59.8	0.591
.019	.043	66.6	.661	.027	.036	64.1	.634
.039	.089	71.8	.714	.037	.049	66.3	.655
.059	.134	76.1	.746	.057	.076	69.4	.686
.084	.191	78.4	.779	.077	.103	72.1	.713
.109	.248	82.0	.814	.107	.143	75.0	.741
.134	.305	84.4	.839	.157	.209	78.9	.780
.159	.361	86.8	.862	.207	.276	82.3	.814
.209	.475	90.9	.902	.257	.343	84.9	.839
.259	.589	93.8	.931	.307	.409	87.5	.865
.309	.703	96.4	.956	.357	.476	89.6	.886
.359	.816	98.0	.974	.407	.544	91.8	.907
.409	.929	99.1	.985	.457	.610	93.7	.926
.459	1.041	99.9	.992	.507	.676	95.4	.943
.509	1.157	100.1	.994	.582	.776	97.4	.963
.584	1.332	100.7	1.000	.657	.876	99.0	.979
.659	1.500	100.7	1.000	.732	.976	100.0	.989
.734	1.669	100.7	1.000	.807	1.076	100.4	.992
				.882	1.177	100.9	.998
				.957	1.275	101.0	.999
				1.032	1.375	101.1	1.000
				1.107	1.478	101.1	1.000
				1.157	1.540	101.1	1.000

TABLE 3.- BOUNDARY-LAYER VELOCITY PROFILE DATA TAKEN WITH PITOT-STATIC PROBE FOR RUNS OF 100 FEET PER SECOND - Continued

(c) 3/8-inch-diameter rod

Station 3 ($Re = 1 \times 10^6$)				Station 4 ($Re = 2 \times 10^6$)			
y	y/δ	$\bar{U}$	$\bar{U}/\bar{U}_\infty$	y	y/δ	$\bar{U}$	$\bar{U}/\bar{U}_\infty$
0.014	0.023	65.7	0.664	0.014	0.015	61.4	0.615
.019	.031	67.9	.686	.019	.020	63.6	.637
.029	.048	70.9	.716	.024	.025	65.5	.656
.039	.064	73.5	.743	.029	.031	66.7	.668
.059	.097	77.1	.780	.039	.041	68.5	.686
.084	.138	80.5	.814	.049	.052	70.5	.706
.109	.179	83.0	.839	.059	.062	71.8	.719
.134	.220	85.3	.862	.074	.078	74.0	.741
.159	.261	87.2	.881	.089	.094	75.4	.754
.209	.343	89.9	.898	.114	.120	77.6	.777
.259	.425	92.1	.931	.139	.146	79.5	.796
.309	.507	93.5	.945	.189	.199	82.5	.826
.384	.630	95.4	.964	.239	.252	85.0	.851
.459	.752	96.5	.975	.289	.304	87.5	.876
.534	.875	97.5	.985	.339	.357	89.1	.892
.609	.998	98.0	.990	.389	.410	90.8	.909
.684	1.121	98.4	.994	.439	.462	92.2	.923
.759	1.244	98.6	.996	.489	.515	93.5	.935
.834	1.369	98.8	.998	.564	.594	94.9	.950
.909	1.493	98.9	.999	.639	.673	96.0	.961
.984	1.617	99.0	1.000	.714	.751	97.0	.971
1.059	1.739	99.0	1.000	.789	.830	97.7	.978
1.159	1.900	99.0	1.000	.864	.910	98.4	.985
				.939	.989	98.9	.990
				1.014	1.069	99.3	.994
				1.089	1.147	99.5	.996
				1.139	1.200	99.7	.998
				1.189	1.254	99.8	.999
				1.239	1.305	99.9	1.000
				1.264	1.335	99.9	1.000

TABLE 3.- BOUNDARY-LAYER VELOCITY PROFILE DATA TAKEN WITH PITOT-STATIC PROBE FOR RUNS OF 100 FEET PER SECOND - Continued

(d) 1/2-inch-diameter rod

Station 3 ($Re = 1 \times 10^6$)				Station 4 ($Re = 2 \times 10^6$)			
y	y/δ	$\bar{U}$	$\bar{U}/\bar{U}_\infty$	y	y/δ	$\bar{U}$	$\bar{U}/\bar{U}_\infty$
0.014	0.025	68.1	0.679	0.014	0.016	61.5	0.623
.017	.030	69.7	.696	.019	.021	63.7	.645
.022	.039	72.0	.719	.024	.027	65.8	.666
.027	.048	73.5	.734	.034	.038	68.0	.688
.037	.066	75.9	.758	.044	.049	70.0	.708
.062	.111	80.2	.801	.064	.072	72.8	.737
.087	.155	83.6	.835	.089	.100	75.9	.768
.112	.200	86.5	.863	.114	.128	78.1	.790
.162	.289	89.9	.897	.164	.184	82.3	.833
.212	.378	92.5	.923	.214	.240	84.5	.855
.262	.468	94.4	.942	.264	.297	86.4	.874
.312	.557	95.8	.956	.314	.353	88.5	.895
.362	.646	96.9	.967	.364	.409	90.1	.912
.412	.736	97.6	.973	.414	.465	91.4	.923
.462	.825	98.4	.981	.464	.521	92.5	.936
.512	.915	98.9	.986	.539	.606	93.9	.951
.562	1.003	99.4	.991	.614	.690	95.0	.962
.612	1.095	99.5	.992	.689	.774	96.1	.973
.662	1.181	99.8	.995	.764	.858	96.9	.981
.712	1.273	99.8	.995	.839	.942	97.2	.984
.762	1.362	100.0	.997	.914	1.027	97.8	.990
.812	1.452	100.3	1.000	.989	1.110	98.2	.994
.862	1.541	100.3	1.000	1.064	1.198	98.3	.995
.912	1.631	100.2	1.000	1.114	1.253	98.5	.997
				1.164	1.310	98.6	.998
				1.214	1.363	98.6	.998
				1.264	1.422	98.7	.999
				1.289	1.450	98.8	1.000

TABLE 3.- BOUNDARY-LAYER VELOCITY PROFILE DATA TAKEN WITH PITOT-STATIC PROBE FOR RUNS OF 100 FEET PER SECOND - Concluded

(e) 3/4-inch-diameter rod

Station 3 ($Re = 1 \times 10^6$)				Station 4 ($Re = 2 \times 10^6$)			
y	y/δ	$\bar{U}$	$\bar{U}/\bar{U}_\infty$	y	y/δ	$\bar{U}$	$\bar{U}/\bar{U}_\infty$
0.014	0.024	71.2	0.699	0.014	0.016	65.7	0.644
.017	.029	73.5	.722	.017	.019	67.6	.662
.020	.034	74.7	.733	.019	.022	68.3	.669
.023	.039	75.7	.744	.022	.025	69.5	.681
.027	.046	77.2	.757	.024	.027	70.3	.689
.032	.054	78.5	.771	.027	.031	71.1	.697
.037	.063	74.5	.781	.029	.033	71.5	.701
.042	.071	80.6	.791	.032	.036	72.2	.708
.047	.080	81.7	.802	.034	.039	72.7	.712
.057	.097	83.1	.816	.037	.042	73.4	.719
.067	.114	84.8	.833	.039	.044	73.6	.721
.077	.131	86.0	.844	.042	.048	74.4	.729
.087	.147	87.1	.855	.047	.052	75.2	.737
.112	.190	89.4	.878	.052	.059	76.0	.745
.137	.231	91.3	.896	.057	.065	76.8	.752
.162	.275	92.8	.912	.062	.070	77.7	.762
.187	.317	94.0	.923	.067	.076	78.4	.769
.237	.402	95.8	.941	.072	.082	79.0	.775
.287	.481	97.0	.953	.112	.127	82.7	.811
.337	.571	98.2	.964	.162	.184	86.5	.848
.387	.656	98.8	.971	.212	.241	89.0	.873
.462	.784	99.9	.981	.262	.298	91.1	.894
.512	.869	100.4	.986	.312	.354	92.8	.910
.562	.954	100.6	.987	.362	.411	94.0	.921
.612	1.039	101.0	.992	.412	.468	95.4	.935
.662	1.123	101.2	.993	.462	.525	96.5	.946
.712	1.206	101.4	.996	.512	.582	97.4	.955
.762	1.295	101.6	.997	.562	.639	98.0	.961
.812	1.377	101.6	.997	.612	.695	98.6	.967
.862	1.462	101.8	1.000	.662	.751	99.3	.974
.912	1.546	101.8	1.000	.712	.810	99.7	.978
.962	1.632	101.8	1.000	.762	.865	100.2	.983
1.012	1.717	101.8	1.000	.812	.924	100.6	.985
				.862	.980	100.9	.989
				.912	1.037	101.1	.991
				.962	1.093	101.5	.995
				1.012	1.151	101.5	.995
				1.062	1.207	101.7	.997
				1.112	1.262	102.0	1.000
				1.162	1.321	102.0	1.000
				1.212	1.377	102.0	1.000

TABLE 4.- BOUNDARY-LAYER VELOCITY AND TURBULENCE-INTENSITY PROFILE DATA TAKEN WITH PLATINUM HOT-WIRE-ANEMOMETER PROBE FOR 50-FEET PER-SECOND RUNS AT STATION 4 WITH $Re = 1 \times 10^6$

y	y/δ	$\bar{U}$	$\bar{U}/\bar{U}_\infty$	$u'/\bar{U}$, percent	y	y/δ	$\bar{U}$	$\bar{U}/\bar{U}_\infty$	$u'/\bar{U}$, percent
No rods					1/8-in.-diam. rod				
0.0016	0.002	12.5	0.259	20.27	0.0021	0.003	13.1	0.269	21.44
.0025	.004	13.1	.271	20.79	.0045	.006	16.6	.341	21.94
.0045	.007	15.6	.322	21.43	.0056	.007	25.4	.521	18.25
.0165	.024	27.8	.575	16.24	.0096	.012	26.5	.545	19.11
.0265	.049	28.8	.595	15.87	.0146	.019	28.1	.576	17.14
.0365	.054	29.7	.614	15.60	.0246	.032	29.2	.599	16.77
.0465	.068	31.7	.655	14.21	.0346	.044	30.2	.620	16.80
.0565	.083	32.1	.664	14.02	.0546	.070	32.7	.670	15.74
.0765	.113	34.2	.708	12.60	.0746	.096	33.2	.682	15.66
.0965	.142	34.9	.722	15.78	.1046	.134	33.9	.695	15.54
.1165	.171	34.9	.722	14.41	.1546	.198	36.0	.739	16.15
.1665	.245	37.1	.767	15.46	.2046	.261	37.2	.763	14.72
.2165	.319	38.9	.805	14.99	.3046	.390	39.7	.815	13.64
.2665	.392	38.9	.805	16.15	.4046	.518	40.9	.840	12.25
.3165	.466	41.1	.850	14.70	.5046	.647	43.7	.898	9.53
.3665	.540	41.1	.850	17.43	.6046	.774	45.1	.925	7.86
.4165	.612	44.6	.923	14.65	.7046	.902	46.9	.961	6.83
.5165	.758	44.7	.925	10.62	.8046	1.035	47.8	.980	6.39
.5665	.831	44.6	.923	10.64	.9046	1.163	48.7	1.000	5.25
.6165	.904	46.1	.954	9.17	1.0046	1.342	48.7	1.000	5.24
.7165	1.055	48.4	1.000	10.20	1.1046	1.473	48.7	1.000	5.24
.8165	1.320	48.4	1.000	7.81	1.9046	2.450	50.5	1.035	5.00
.9165	1.482	48.7	1.008	5.73					
1.0165	1.640	48.4	1.000	5.41					
1.1165	1.884	47.5	.983	9.37					
1.2165	1.966	47.5	.983	7.20					
1.8165	2.945	46.9	.970	5.79					
1/2-in.-diam. rod					3/4-in.-diam. rod				
0.0021	0.003	15.8	0.362	21.05	0.0016	0.003	15.1	0.361	13.41
.0036	.006	17.9	.369	19.64	.0036	.006	19.0	.455	17.47
.0056	.009	22.2	.458	19.63	.0056	.010	20.9	.500	17.44
.0086	.014	27.4	.565	18.23	.0086	.015	25.1	.600	15.84
.0136	.022	29.2	.602	17.11	.0136	.024	26.5	.634	15.31
.0186	.030	30.8	.636	16.76	.0236	.042	28.8	.688	14.37
.0236	.038	31.7	.654	16.80	.0336	.059	29.4	.703	13.44
.0336	.054	32.8	.677	15.05	.0536	.095	30.9	.739	13.73
.0436	.070	33.6	.691	15.41	.0736	.130	32.7	.782	12.40
.0586	.094	34.2	.705	15.60	.0936	.166	31.7	.758	12.34
.0786	.127	35.7	.735	15.21	.1136	.201	33.6	.804	11.60
.0986	.159	36.8	.760	15.21	.1636	.289	34.6	.829	11.70
.1286	.207	39.2	.809	15.00	.2136	.376	35.4	.848	11.16
.1586	.255	39.4	.814	14.72	.2636	.465	36.7	.879	10.37
.2086	.335	41.3	.851	14.34	.3136	.552	37.8	.902	10.47
.2586	.416	41.7	.860	13.62	.3636	.641	38.4	.919	10.39
.3086	.496	42.8	.882	13.57	.4136	.731	38.9	.930	9.56
.4086	.658	46.3	.955	12.18	.4636	.820	40.3	.962	9.42
.5086	.818	45.6	.942	11.13	.5136	.909	40.3	.962	9.13
.6086	.979	46.5	.959	9.15	.5636	1.000	41.1	.982	8.93
.7086	1.143	48.5	1.005	8.47	.6136	1.088	39.8	.951	8.64
.8086	1.301	49.4	1.020	8.29	.6636	1.175	41.8	1.000	8.25
.9086	1.463	47.8	.985	7.19	.7136	1.265	41.8	1.000	8.02
1.0086	1.773	48.1	.992	6.53	.7636	1.357	41.8	1.000	7.70
					.8136	1.441	41.8	1.000	7.49
					.9136	1.619	40.0	.959	7.42
					1.1136	2.010	42.7	1.022	6.09

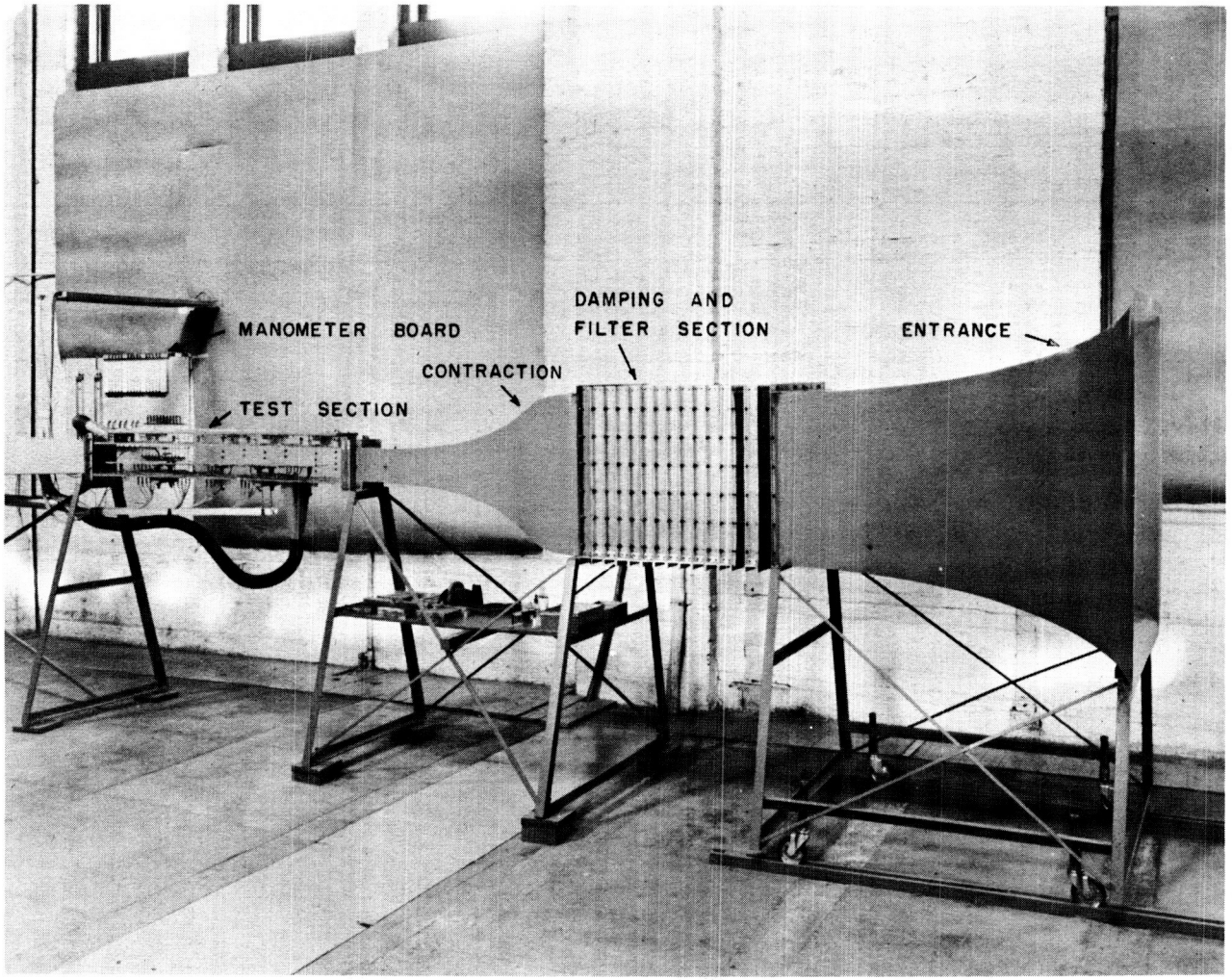

Figure 1.- Variable-turbulence wind tunnel. L-59-6483

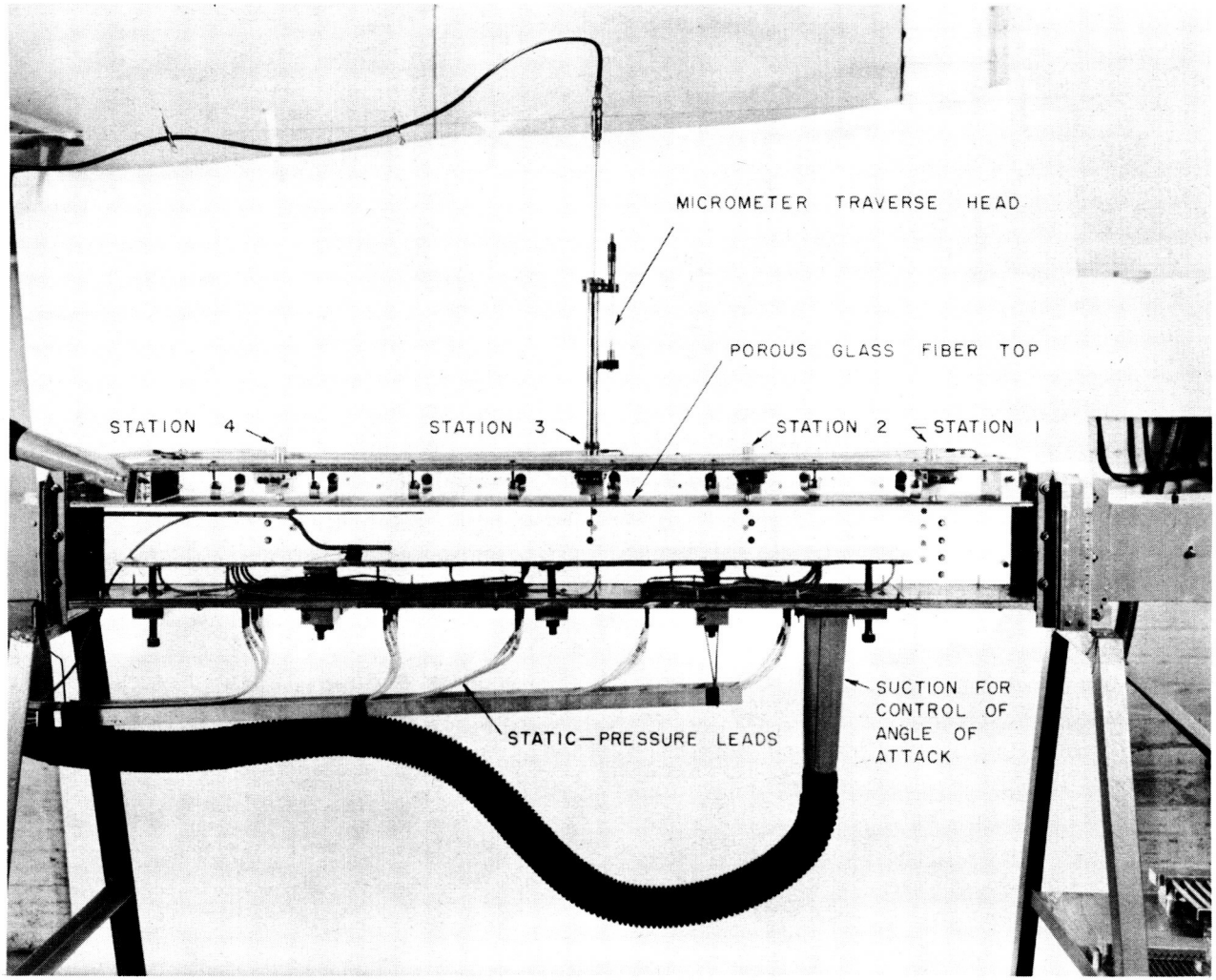

Figure 2.- Test section of variable-turbulence wind tunnel. L-59-6484

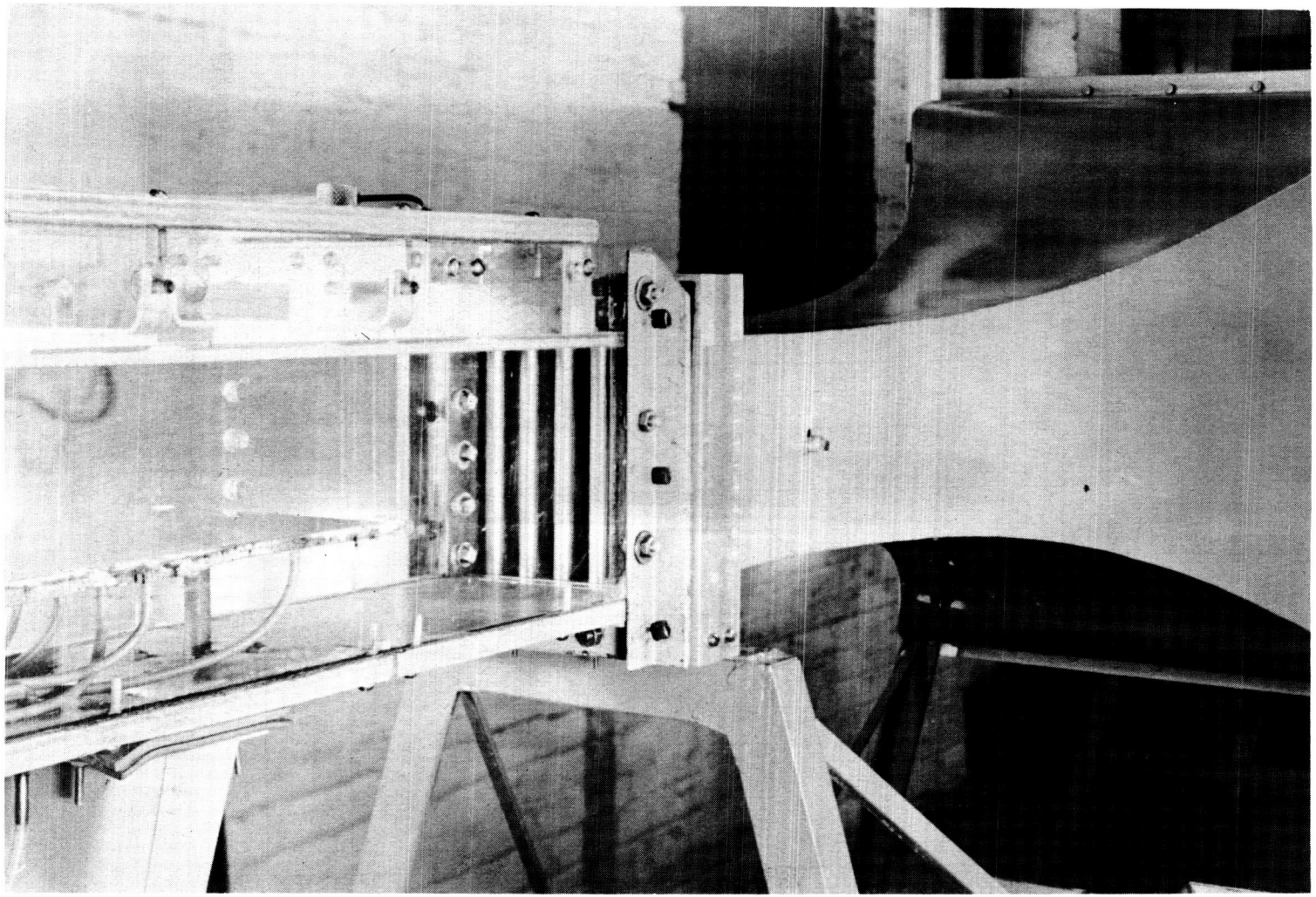

L-59-6485

Figure 3.- View upstream from test section showing turbulence-promoting rods in place.

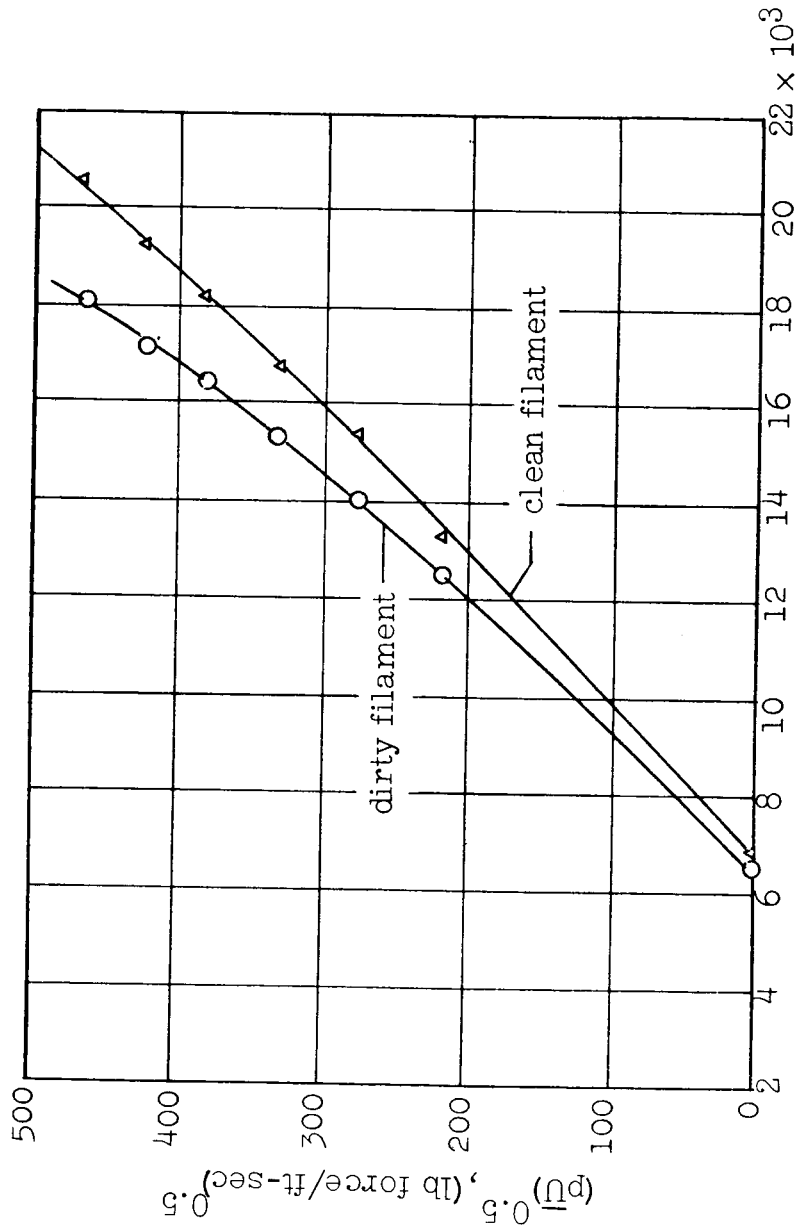

Figure 4.- Tungsten-filament calibration.

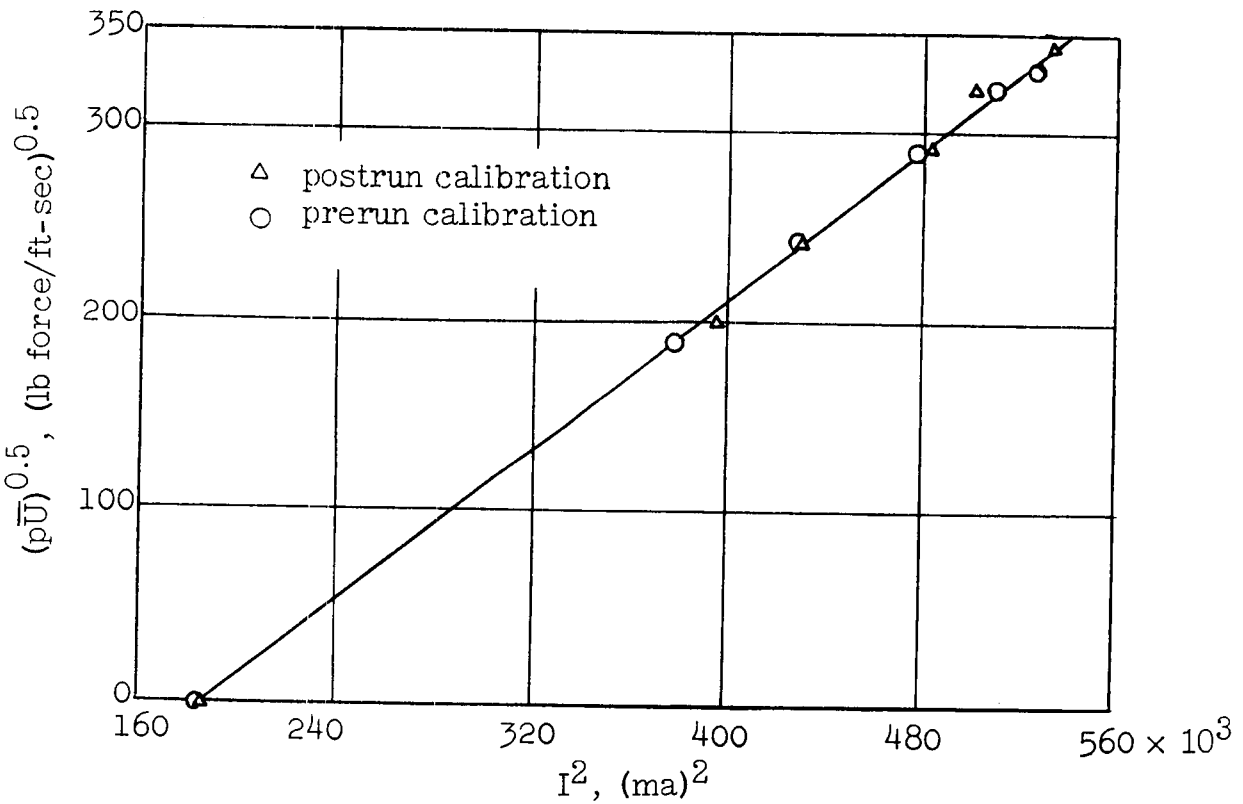

Figure 5.- Platinum-filament calibration.

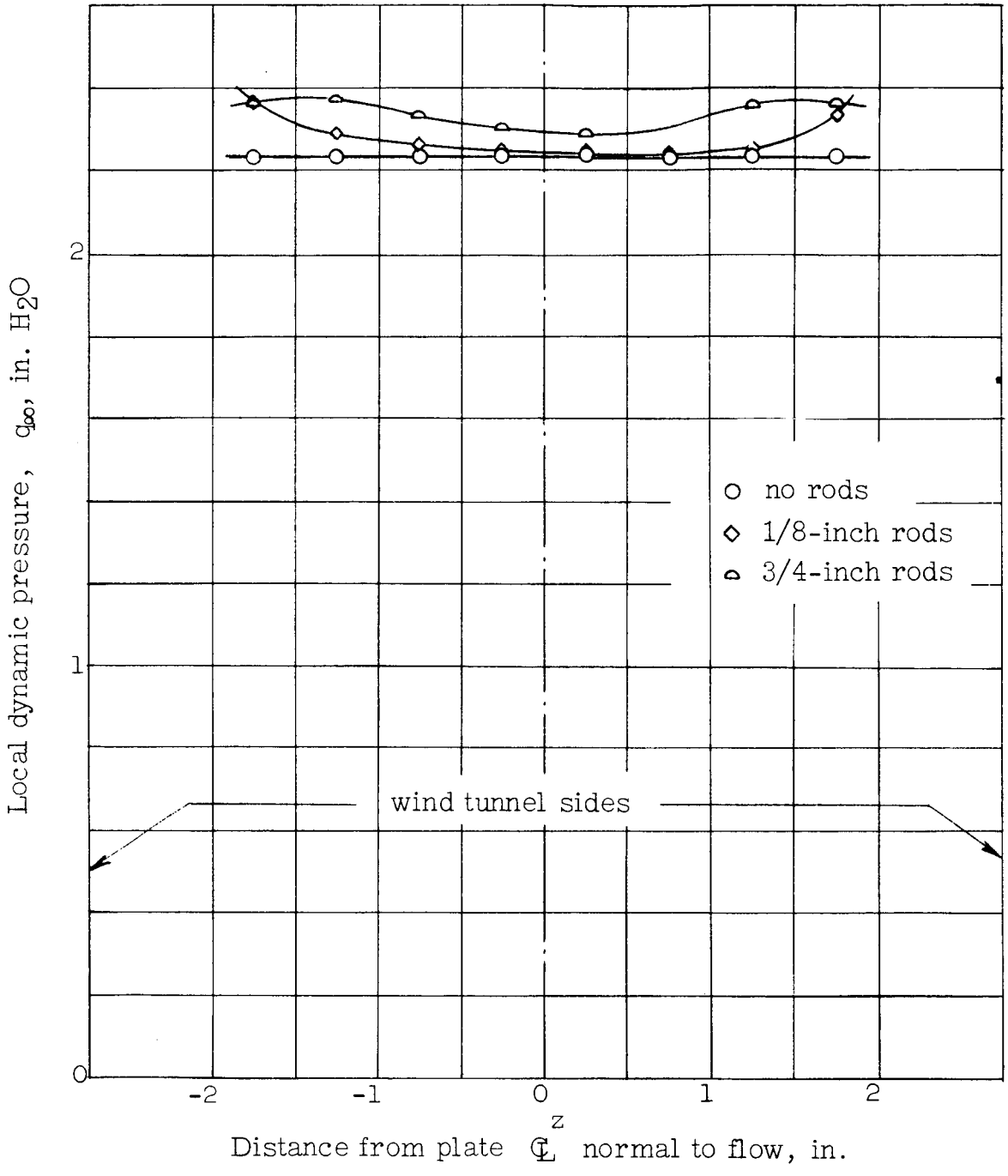

Figure 6.- Horizontal, free-stream, dynamic head profiles. Data taken at station 4, 1 inch above plate.

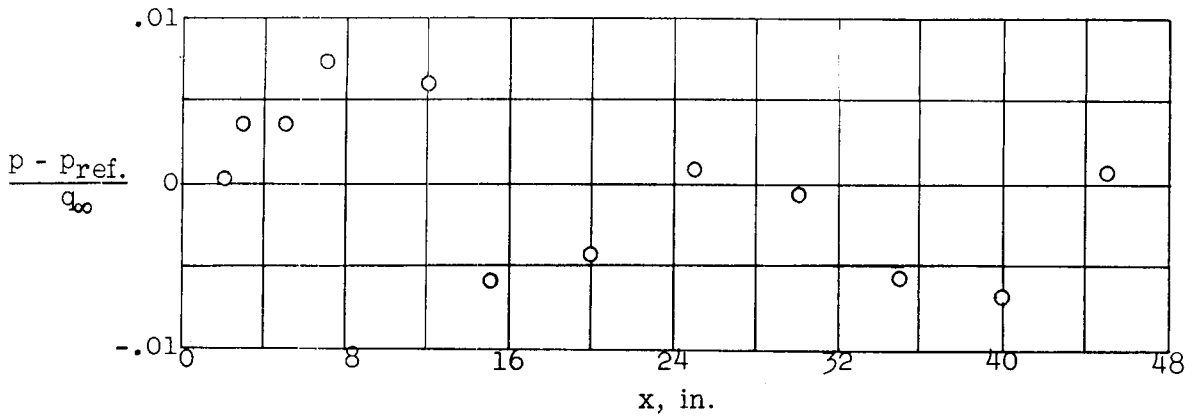

(a) $\bar{U}_\infty$ = 100 feet per second; 1/2-inch rods.

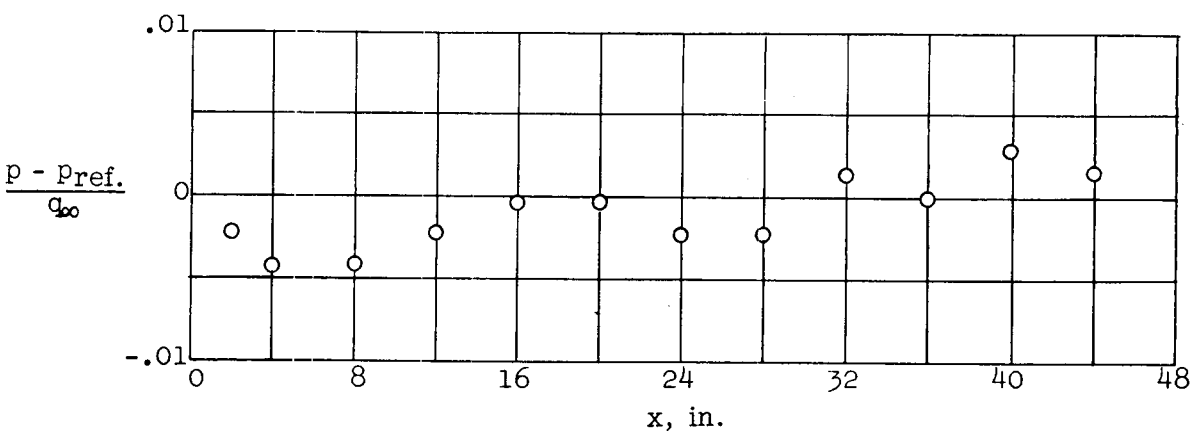

(b) $\bar{U}_\infty$ = 50 feet per second; 3/4-inch rods.

Figure 7.- Longitudinal static-pressure distribution along flat plate.

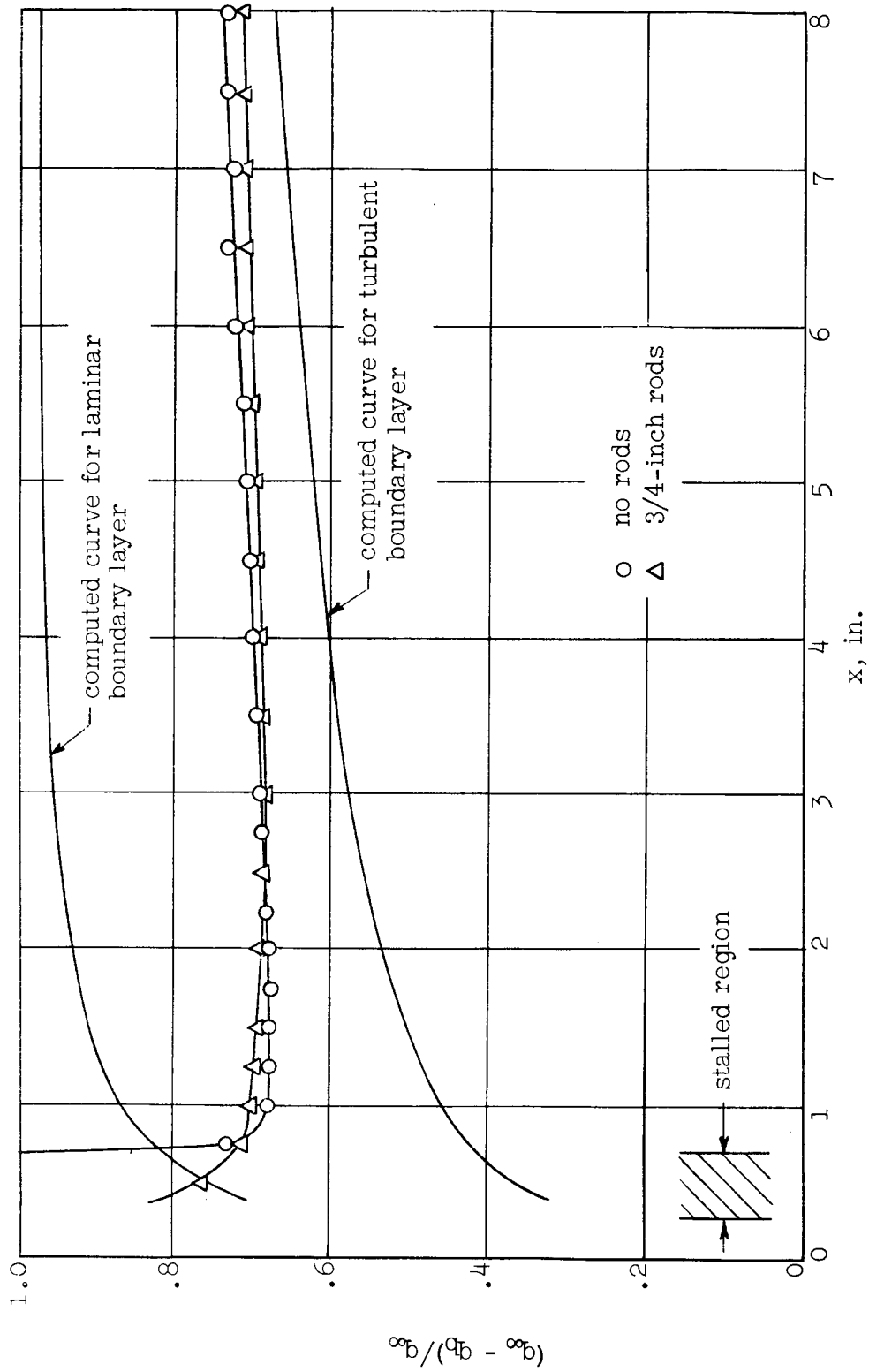

Figure 8.- Transition location found by comparison of computed and experimental curves for $\bar{U}_\infty$ = 100 feet per second. Data taken at $y \approx 0.005$ inch.

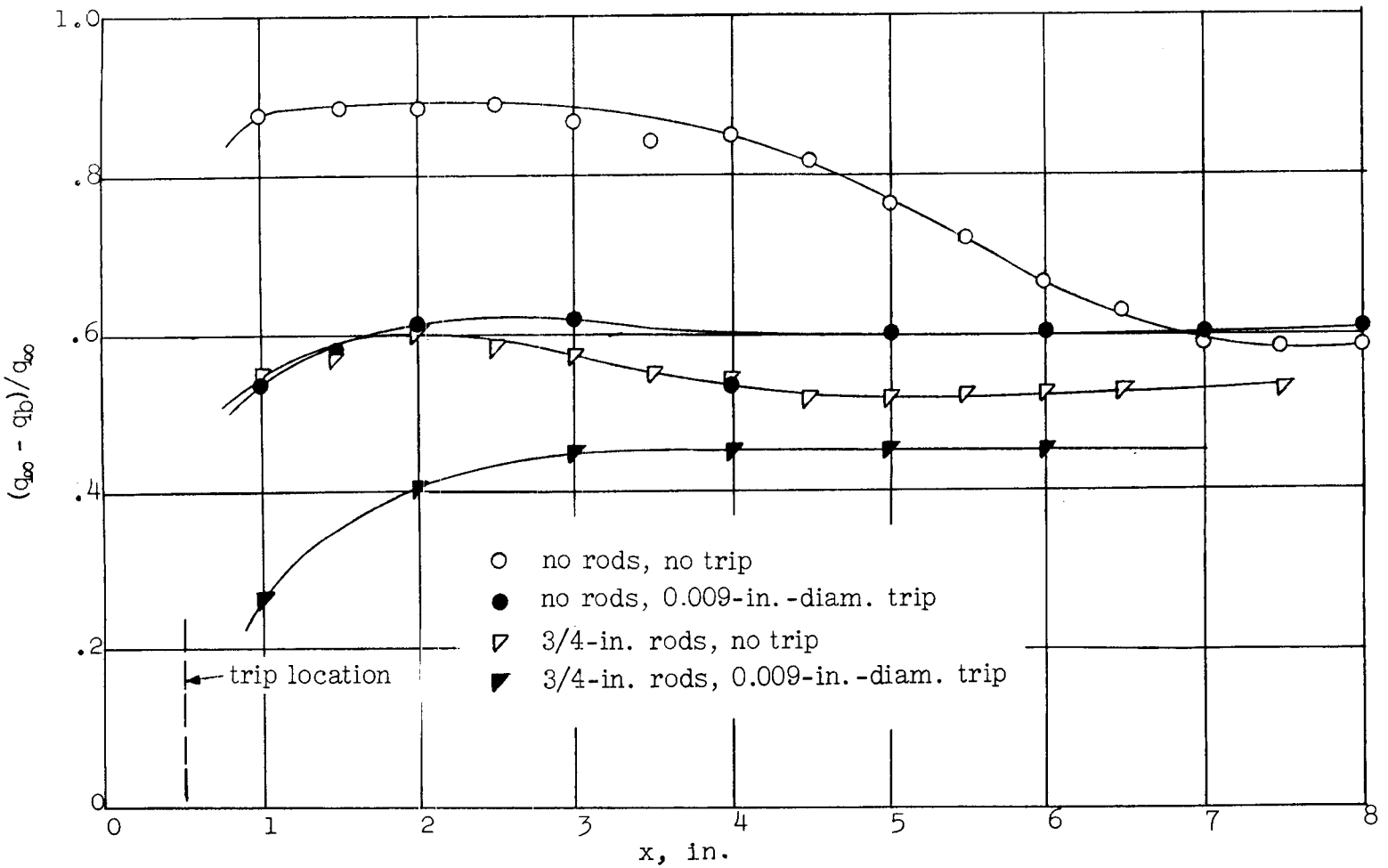

Figure 9.- Comparison of transition location at various turbulence intensities with and without boundary-layer trip. Data taken at $y \approx 0.005$ inch.

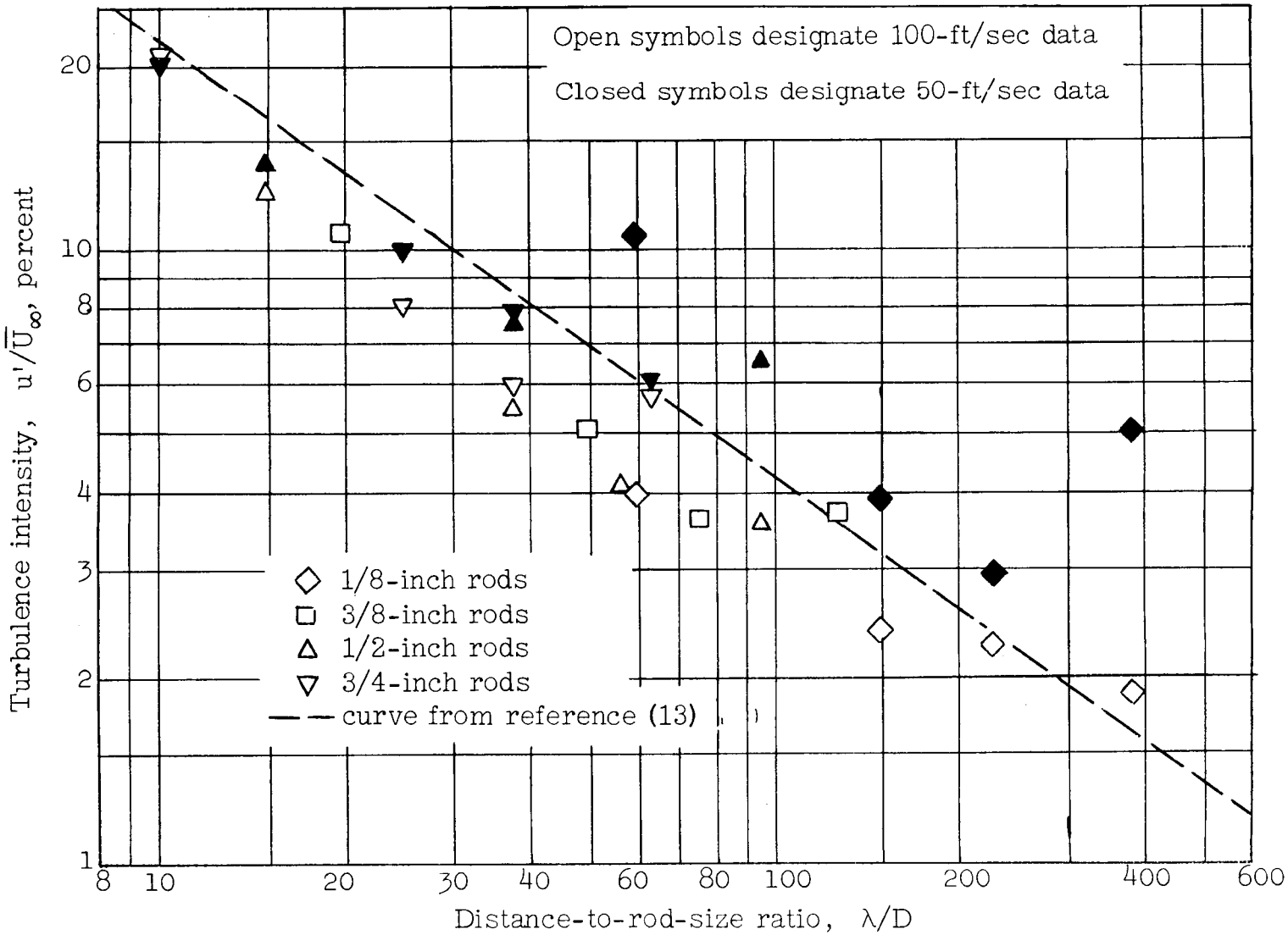

Figure 10.- Turbulence intensity for various rod sizes and distances downstream from rods.

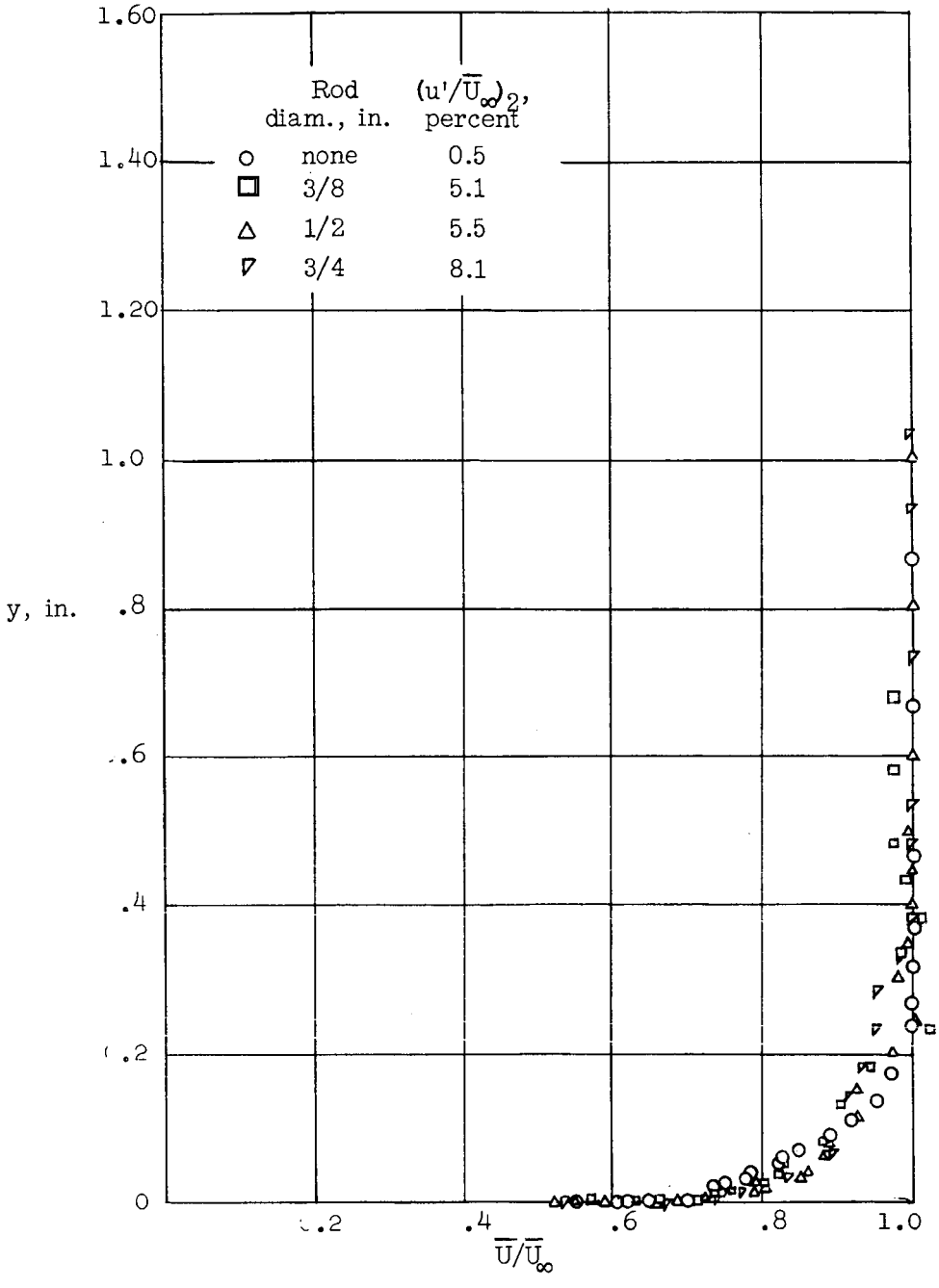

(a) Dimensional profile; station 2; Re = 0.5×10^6.

Figure 11.- Velocity profiles taken with tungsten hot-wire-anemometer probe for runs at 100 feet per second.

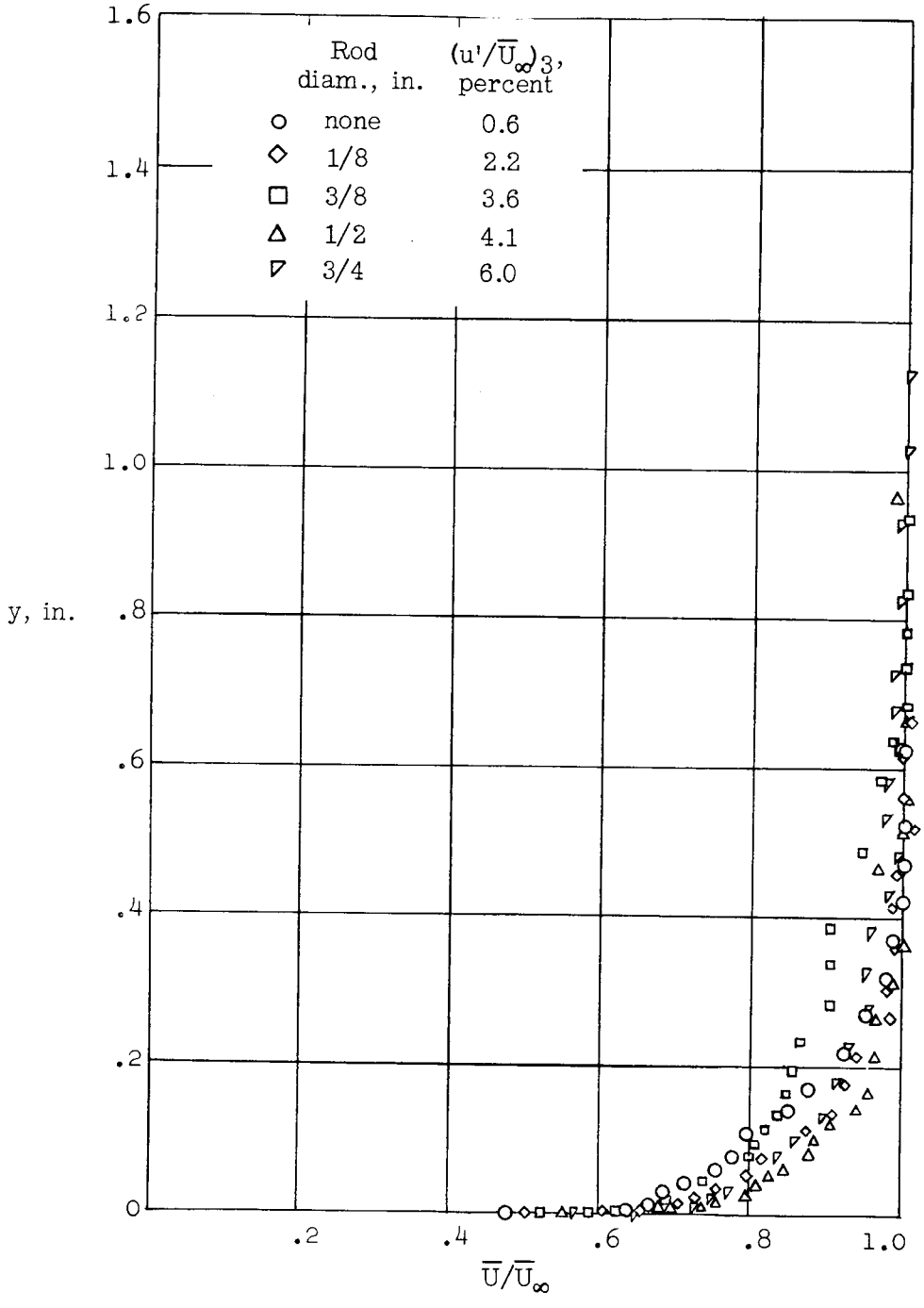

(b) Dimensional profile; station 3; Re = 1×10^6.

Figure 11.- Continued.

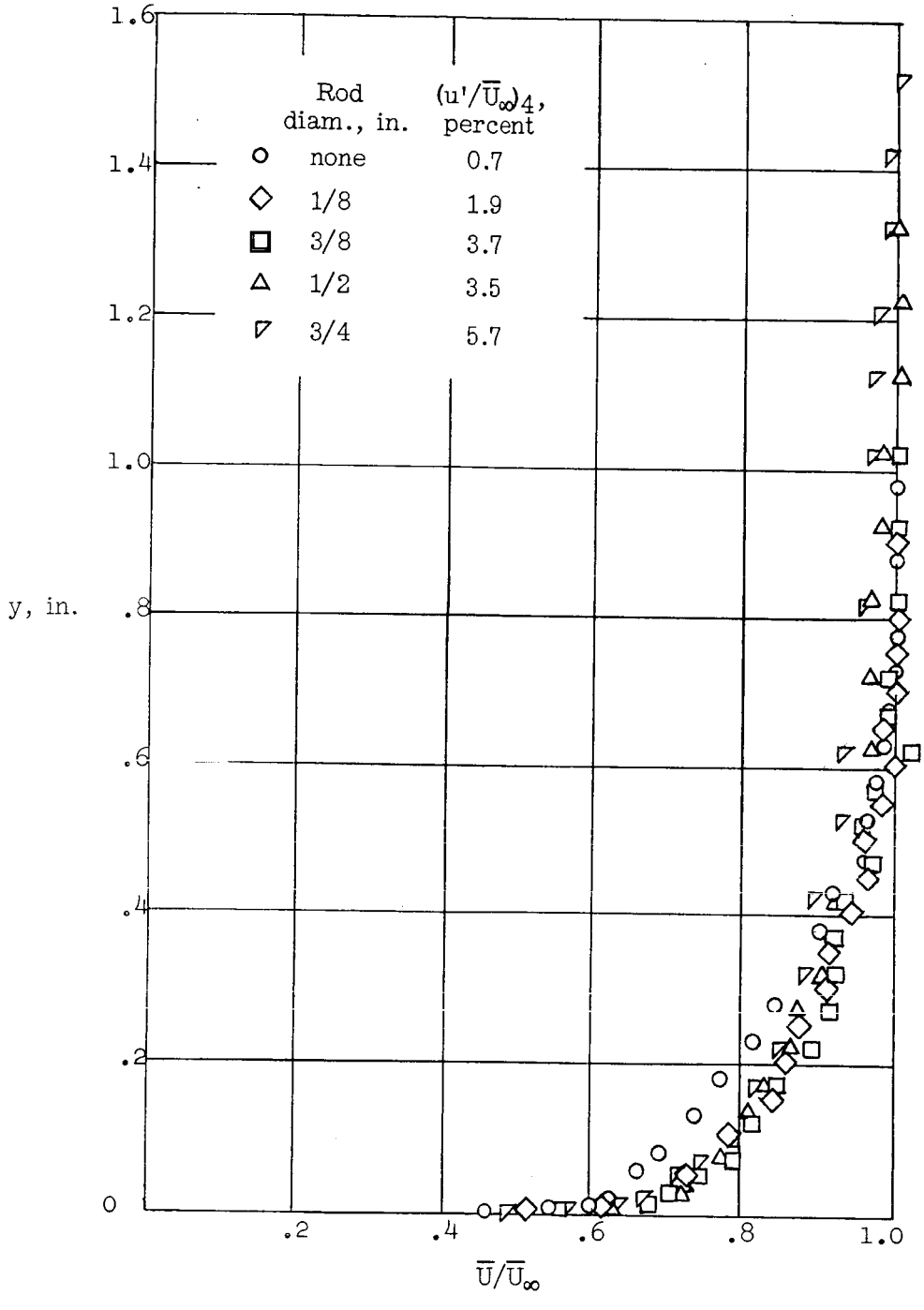

(c) Dimensional profile; station 4; Re = 2×10^6.

Figure 11.- Continued.

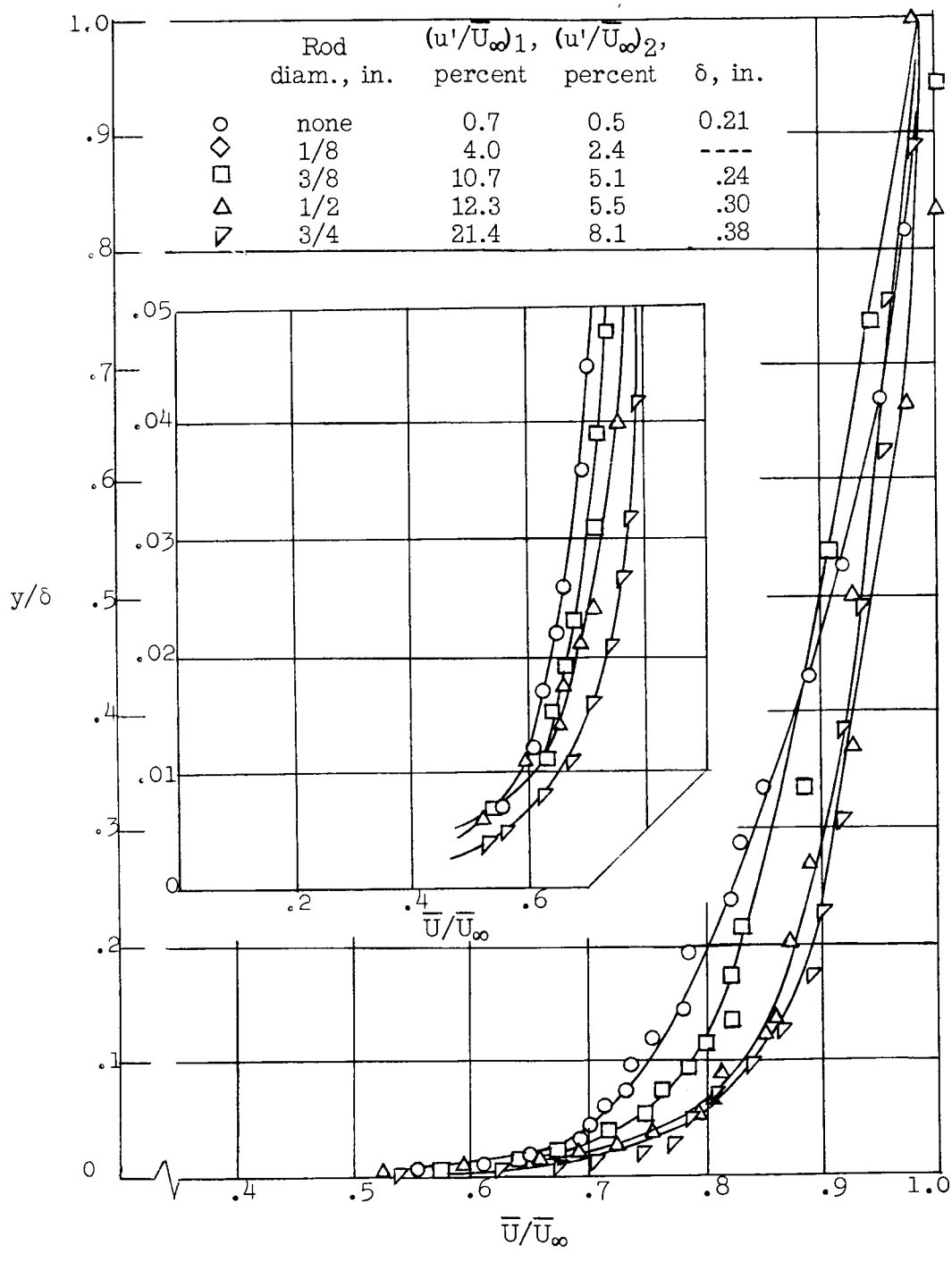

(d) Dimensionless profile; station 2; Re = 0.5×10^6.

Figure 11.- Continued.

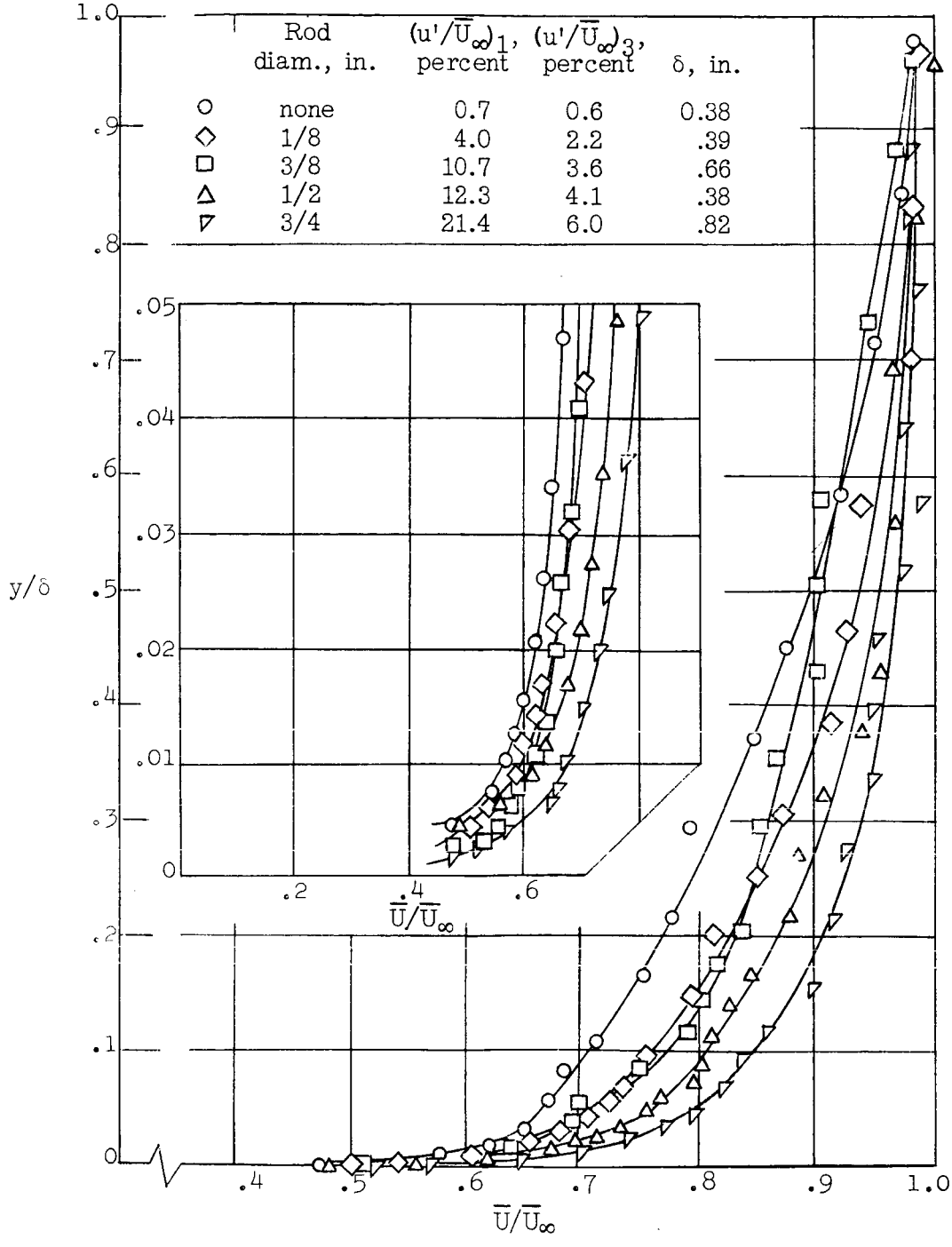

(e) Dimensionless profile; station 3; Re = 1×10^6.

Figure 11.- Continued.

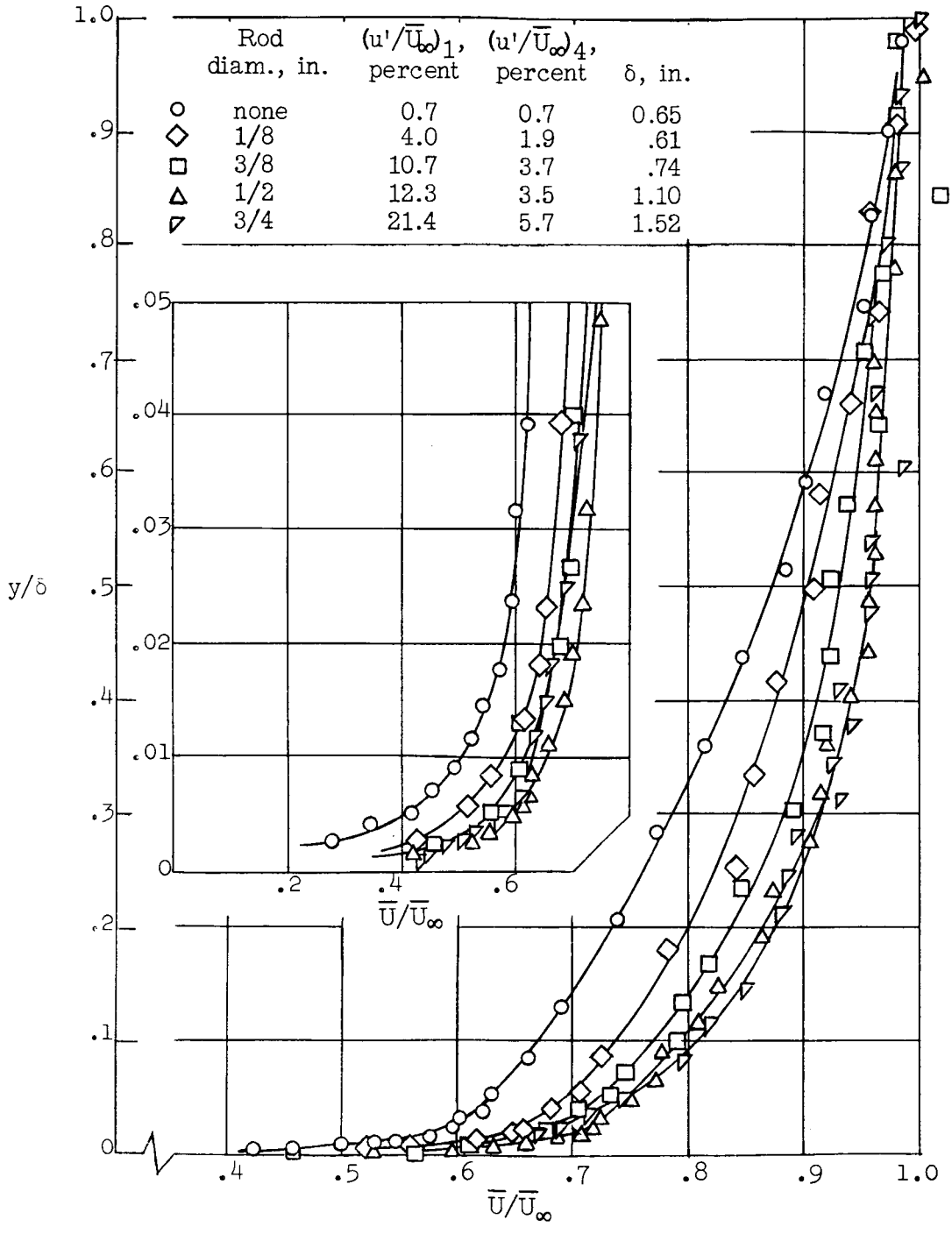

(f) Dimensionless profile; station 4; Re = 2×10^6.

Figure 11.- Concluded.

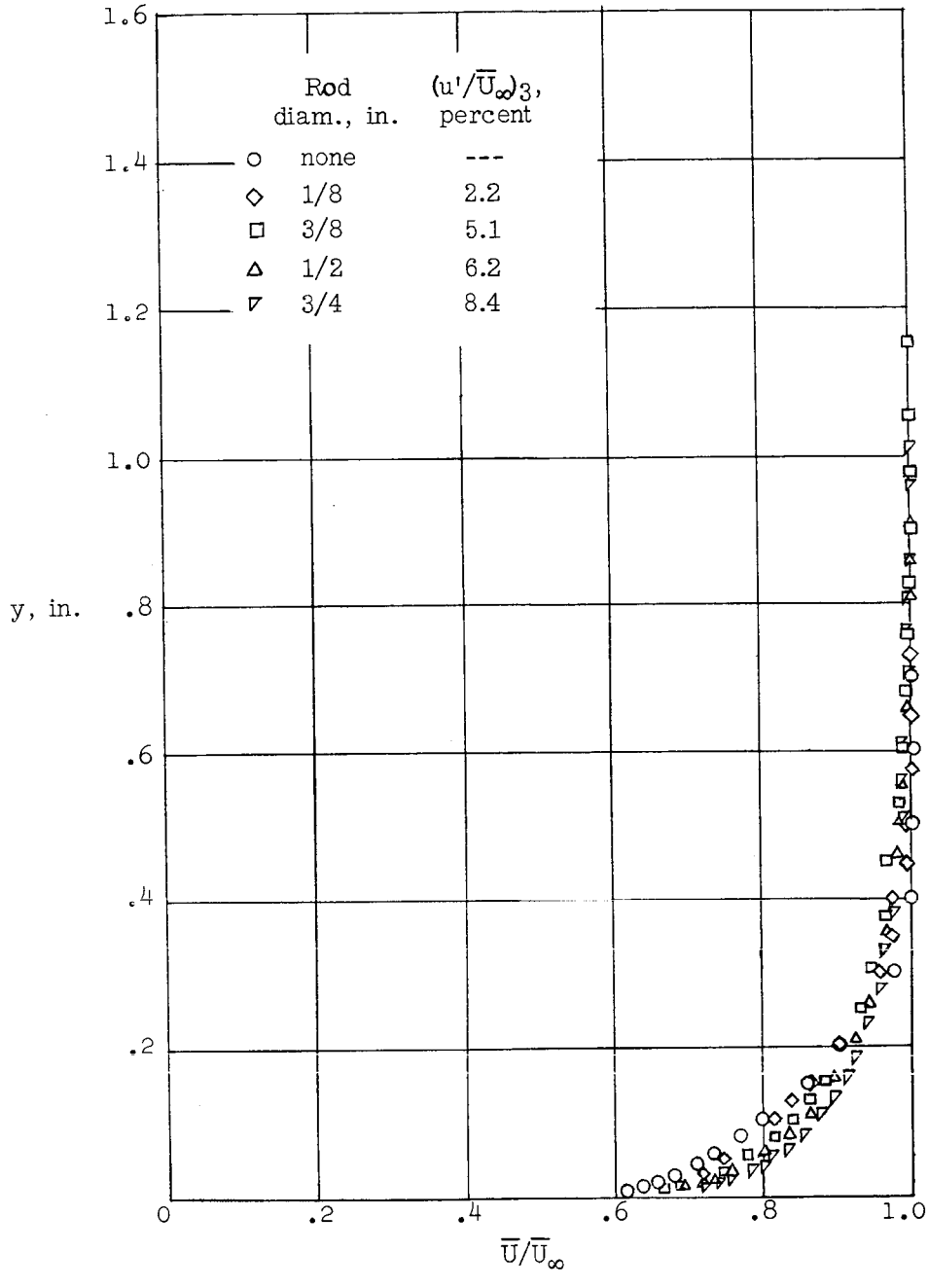

(a) Dimensional profile; station 3; Re = 1×10^6. $(u'/\overline{U}_\infty)_3$ values are taken from line in figure 10.

Figure 12.- Velocity profiles taken with pitot-static probe for runs at 100 feet per second.

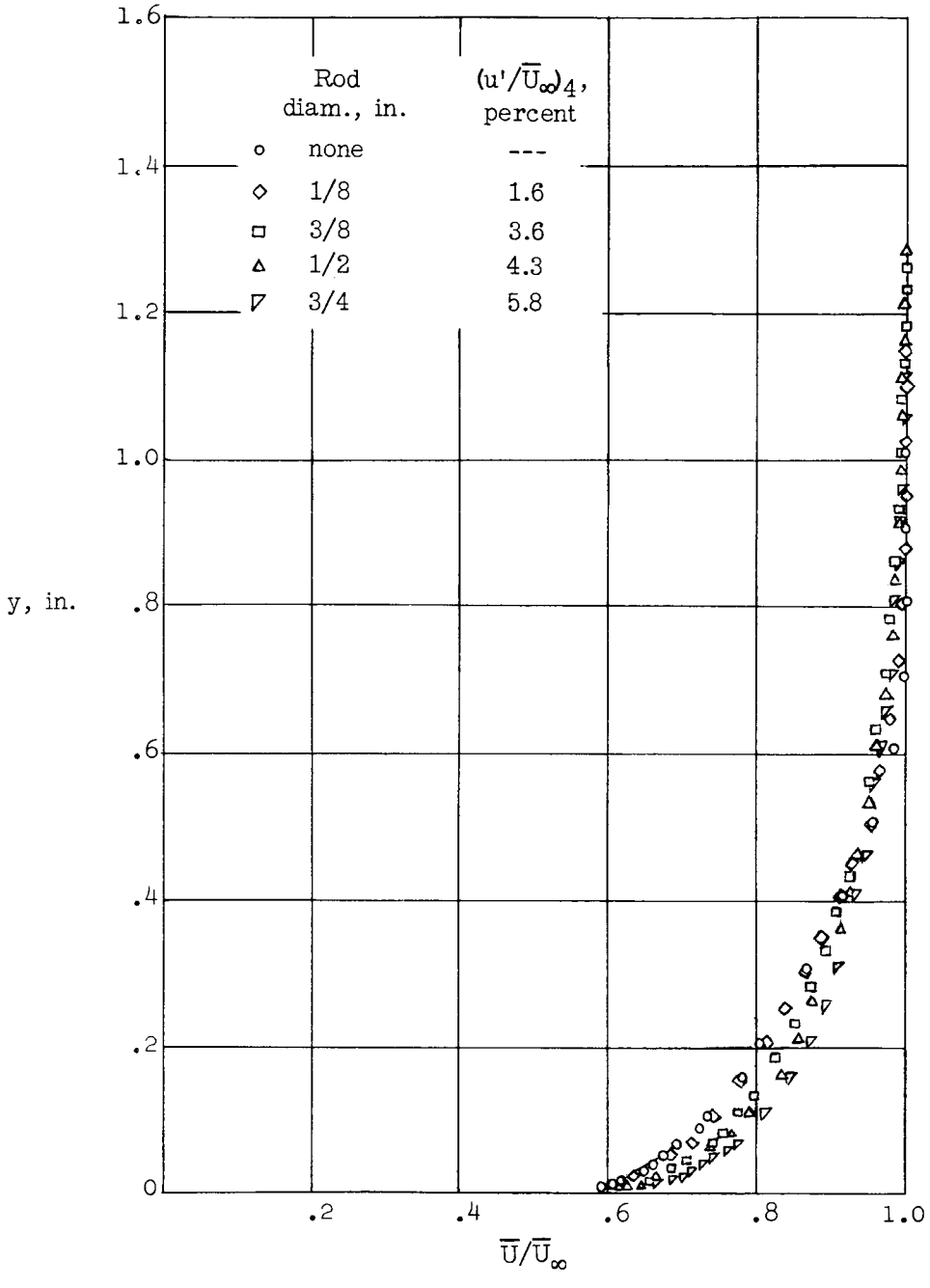

(b) Dimensional profile; station 4; Re = 2×10^6. $\left(u'/\overline{U}_\infty\right)_4$ values are taken from line in figure 10.

Figure 12.- Continued.

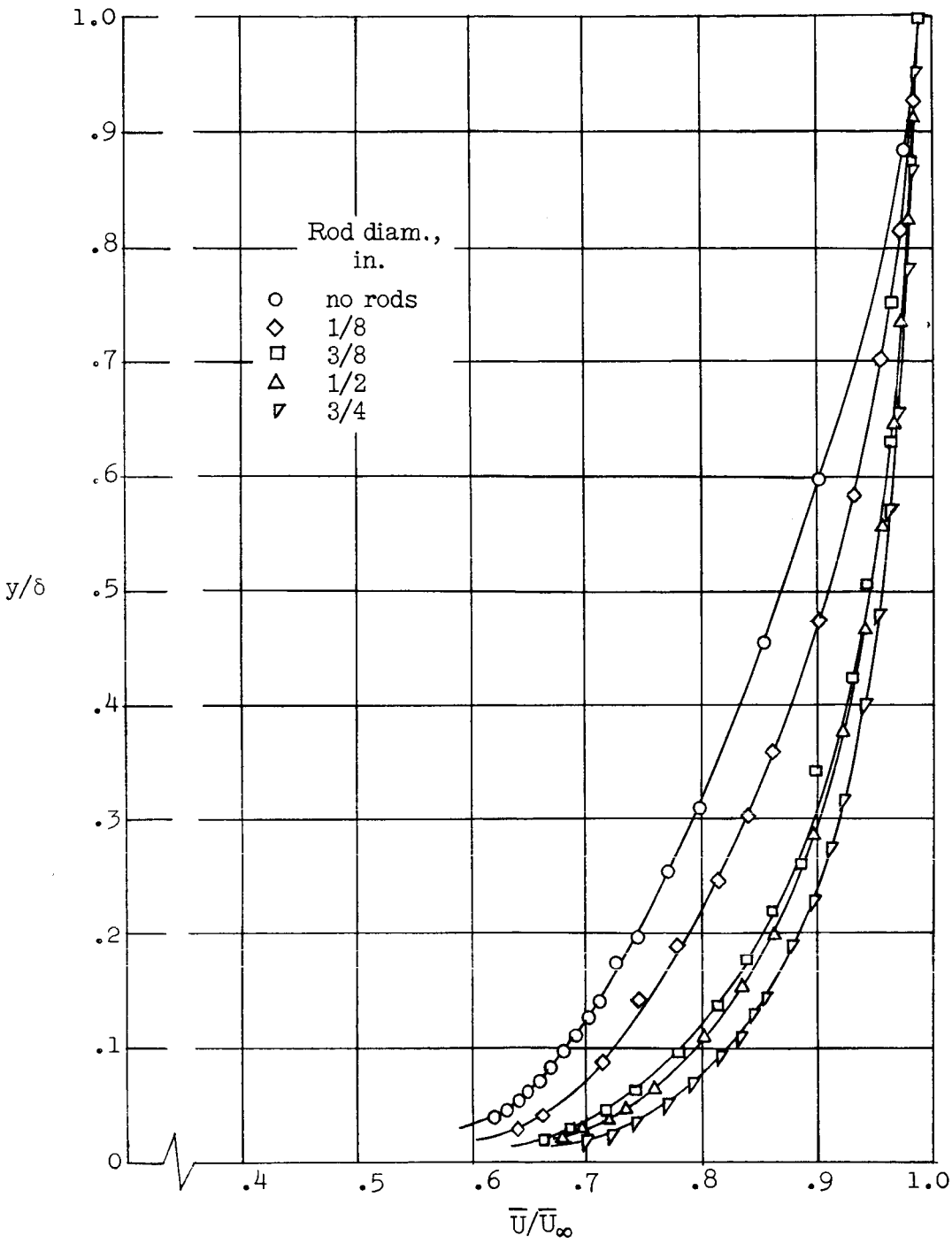

(c) Dimensionless profile; station 3; Re = 1×10^6.

Figure 12.- Continued.

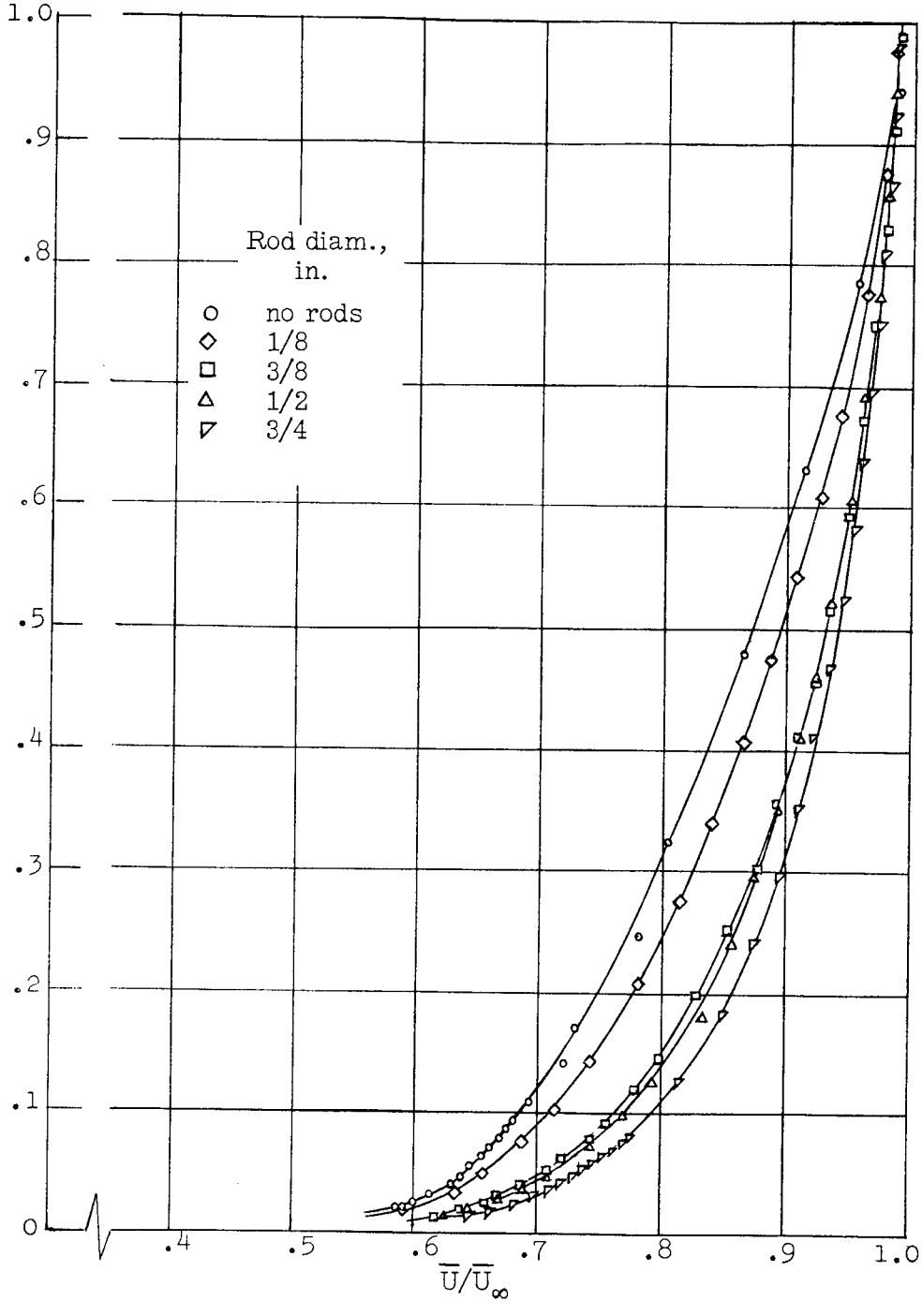

(d) Dimensionless profile; station 4; Re = 2×10^6.

Figure 12.- Concluded.

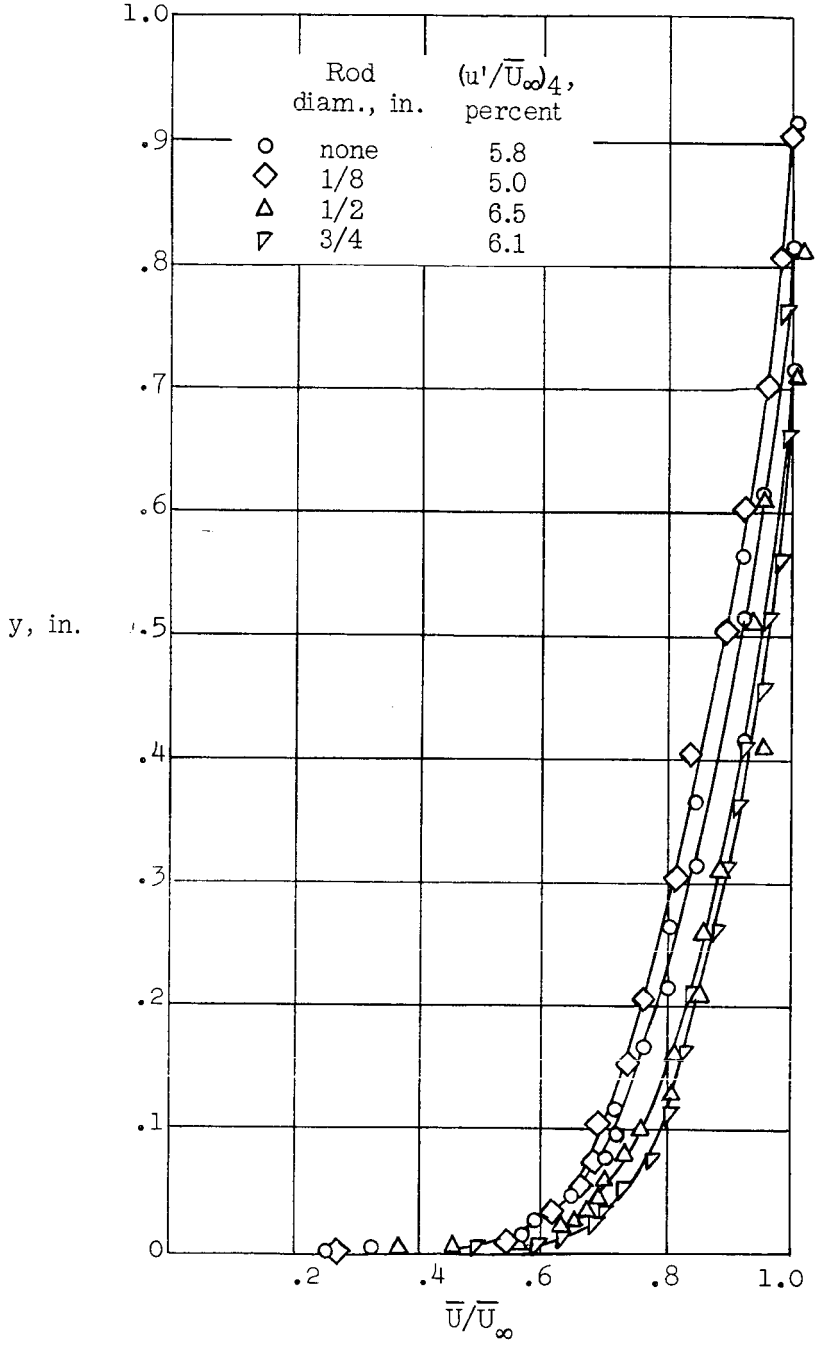

(a) Dimensional profile; station 4; Re = 1×10^6.

Figure 13.- Velocity profiles taken with platinum hot-wire-anemometer probe at runs of 50 feet per second.

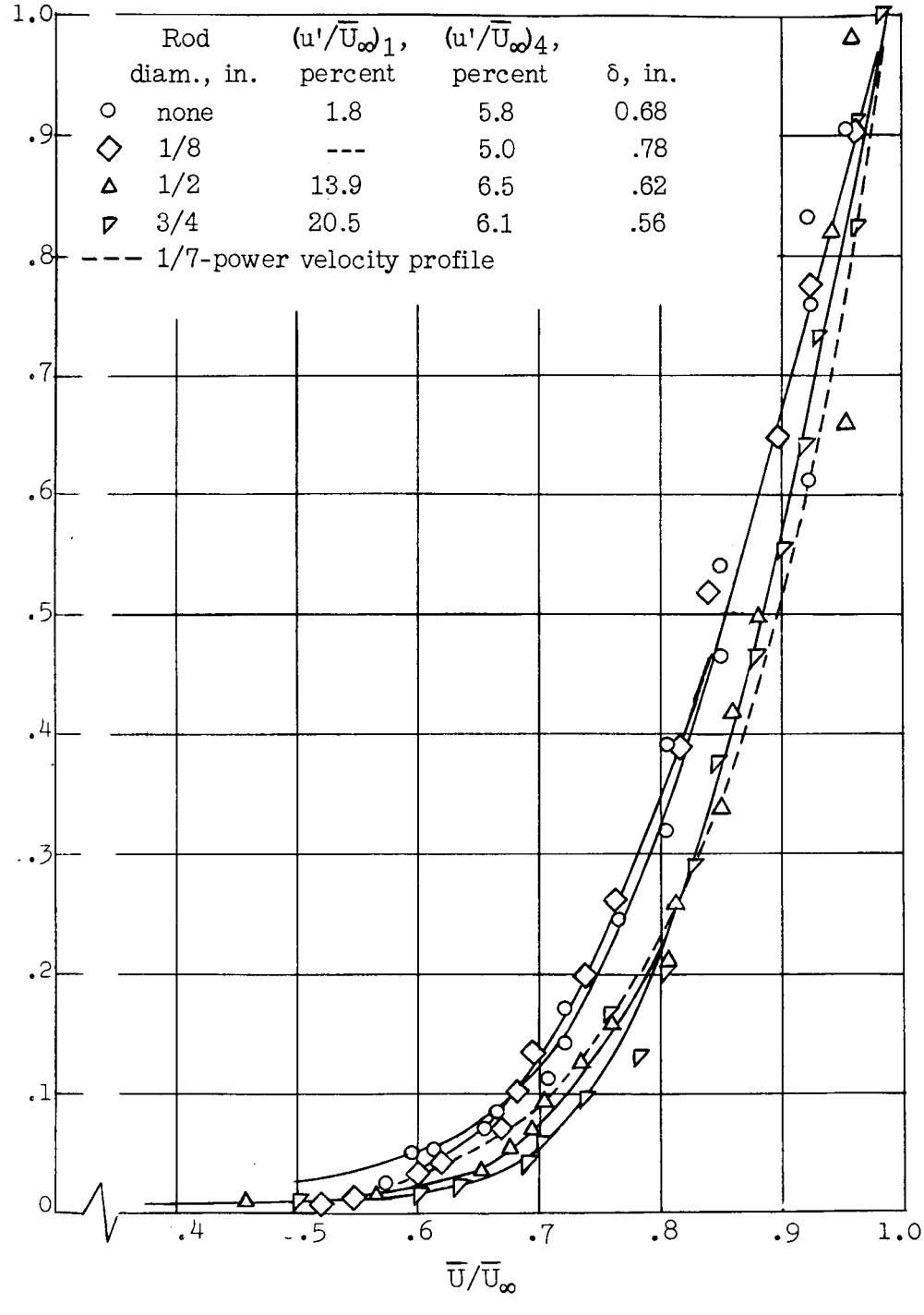

(b) Dimensionless profiles; station 4; Re = 1×10^6.

Figure 13.- Concluded.

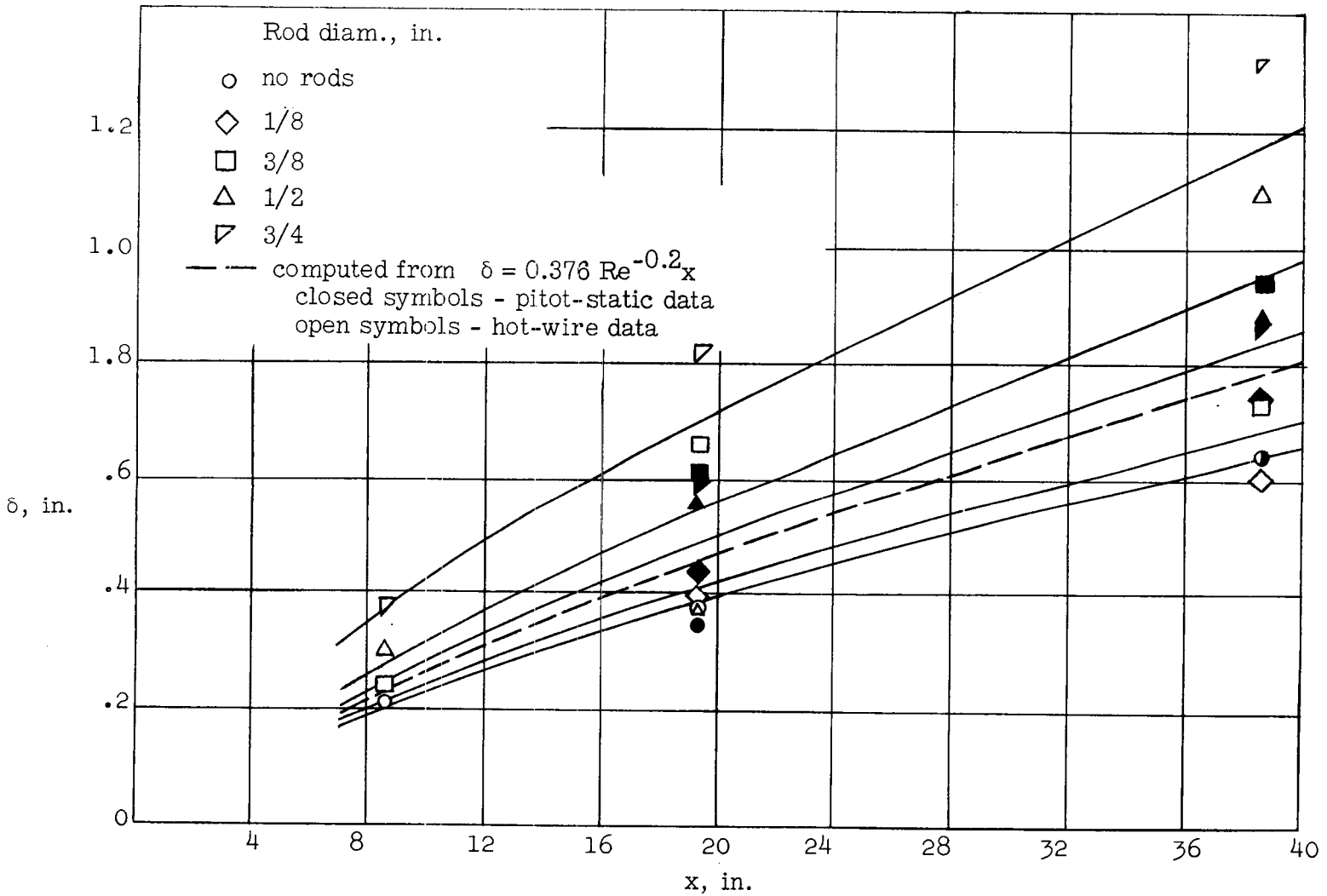

Figure 14.- Turbulent boundary-layer growth on flat plate at various turbulence intensities.

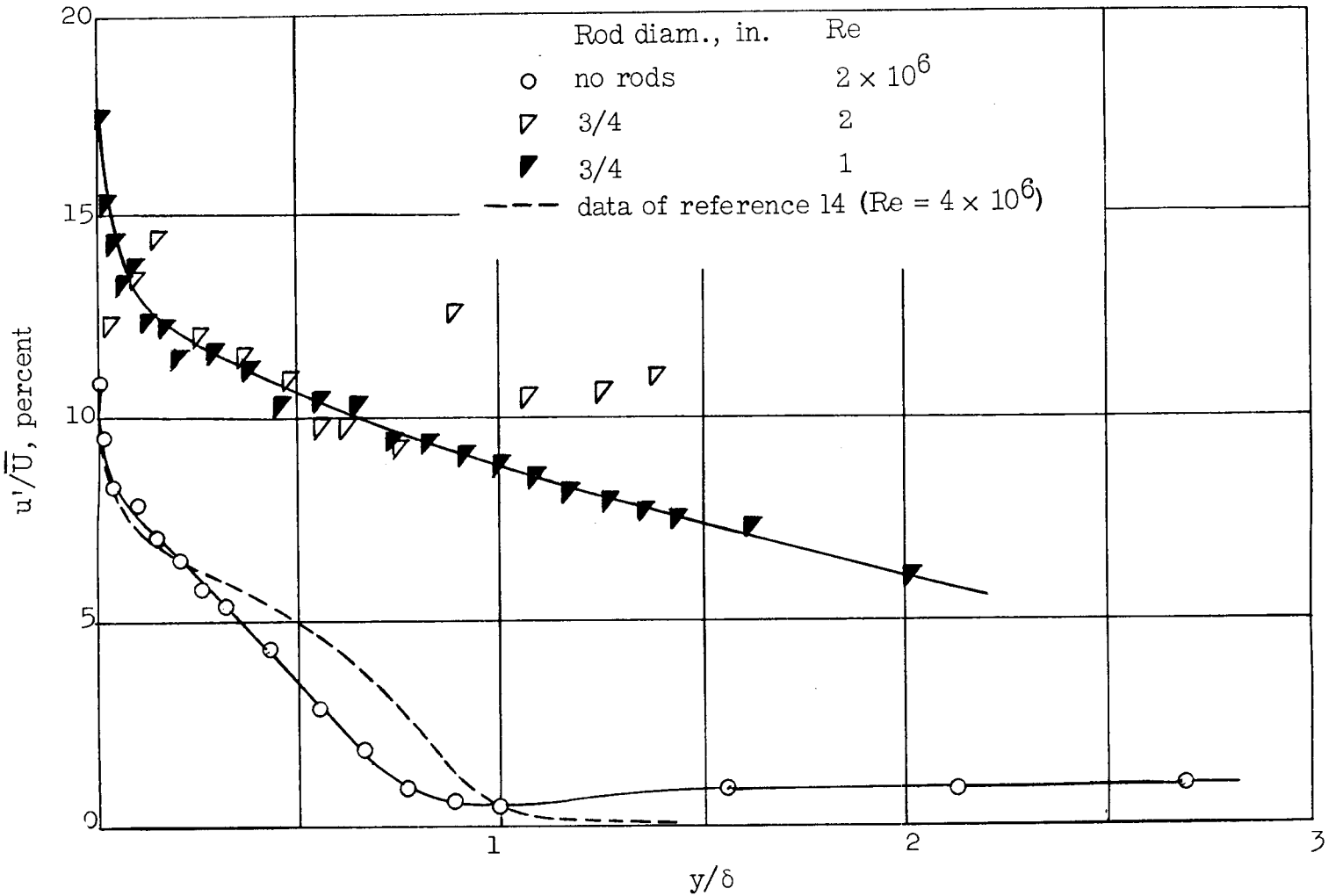

Figure 15.- Turbulence-intensity distribution.

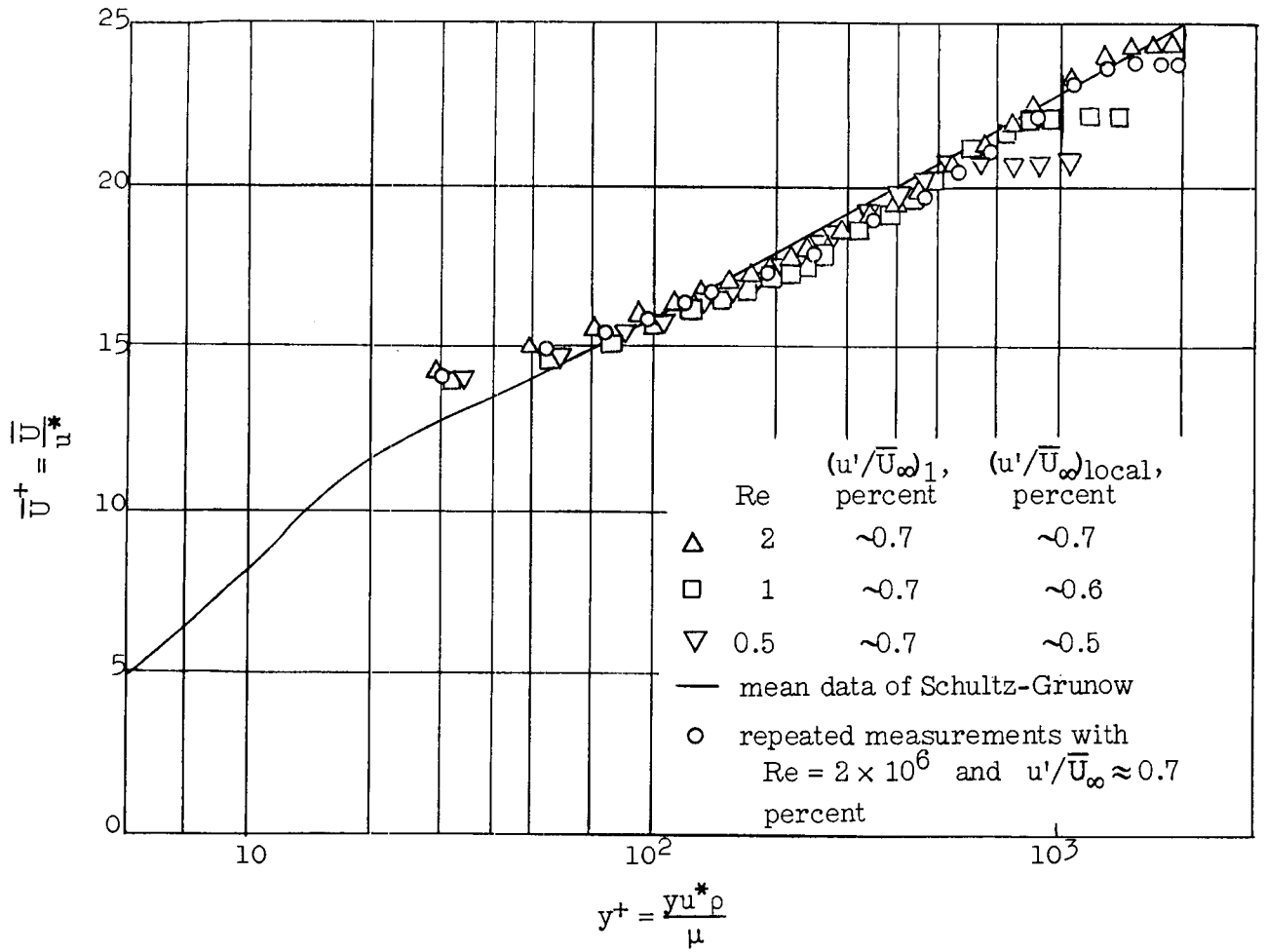

(a) Low turbulence intensities.

Figure 16.- Comparison of velocity-profile data taken in modified tunnel with pitot-static probe with Schultz-Grunow data.

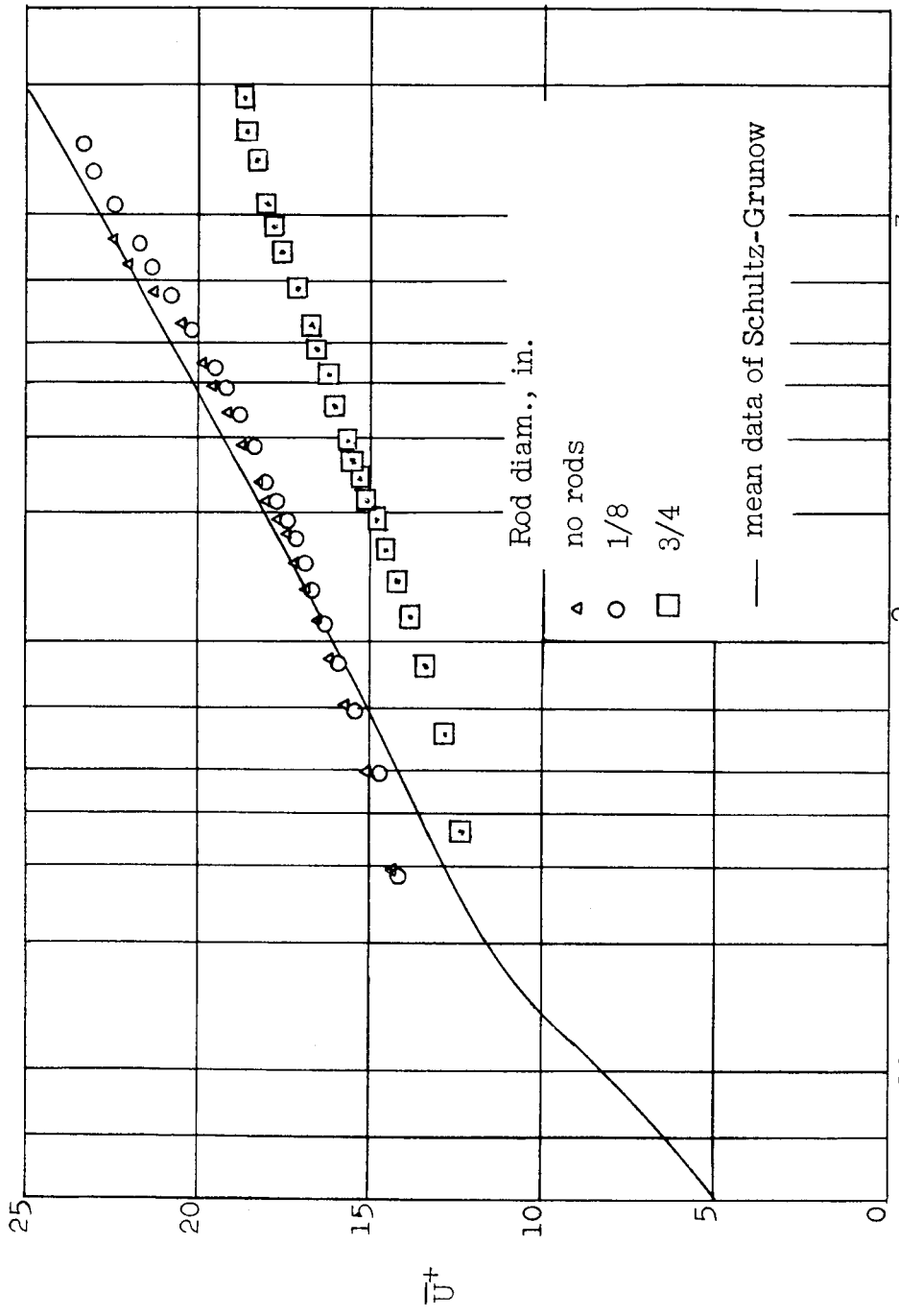

(b) High turbulence intensities. Re = 2×10^6.

Figure 16.- Concluded.

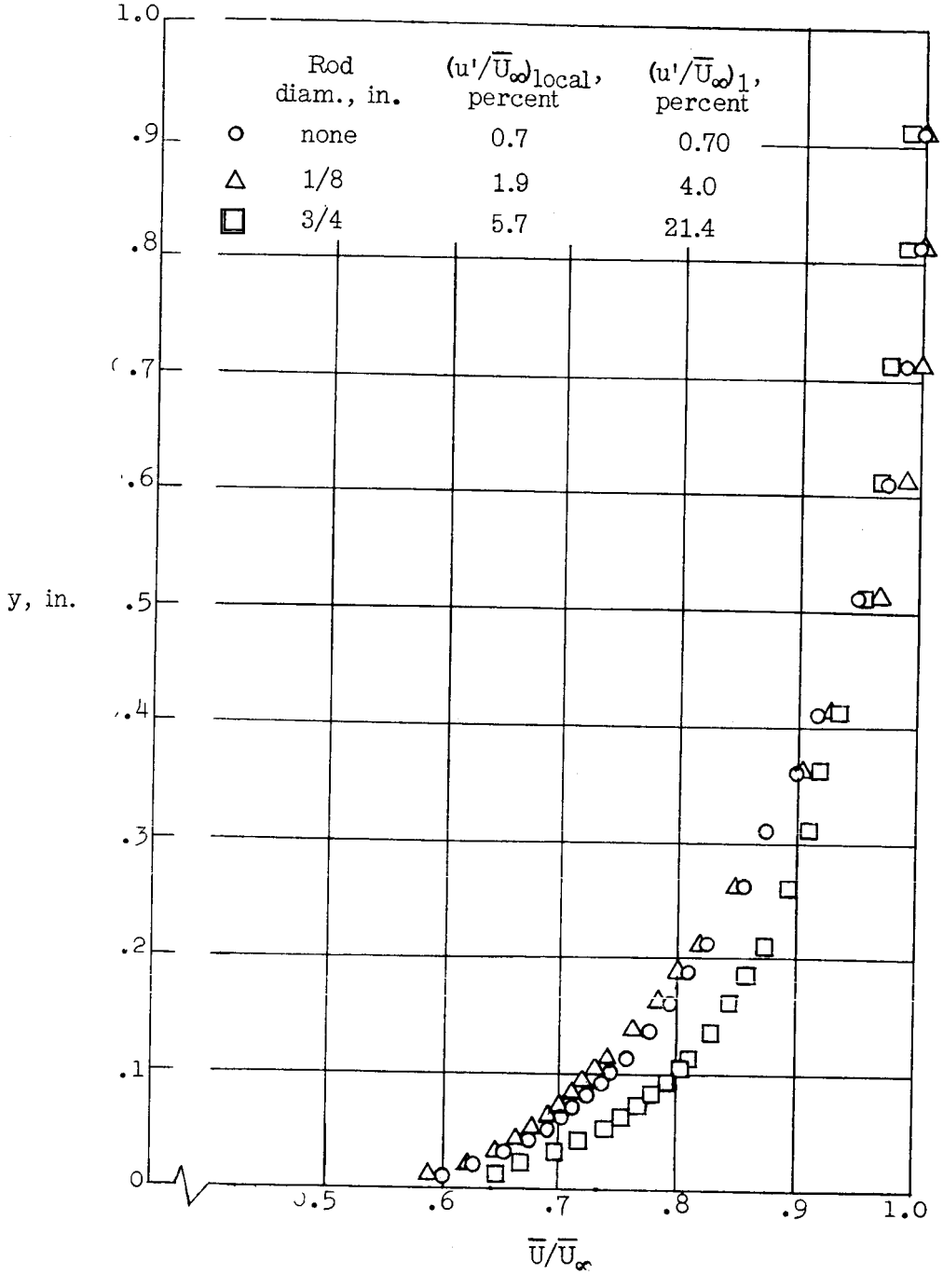

(a) Nondimensional profiles. Re = 2×10^6.

Figure 17.- Velocity profiles taken with pitot-static probe in modified tunnel.

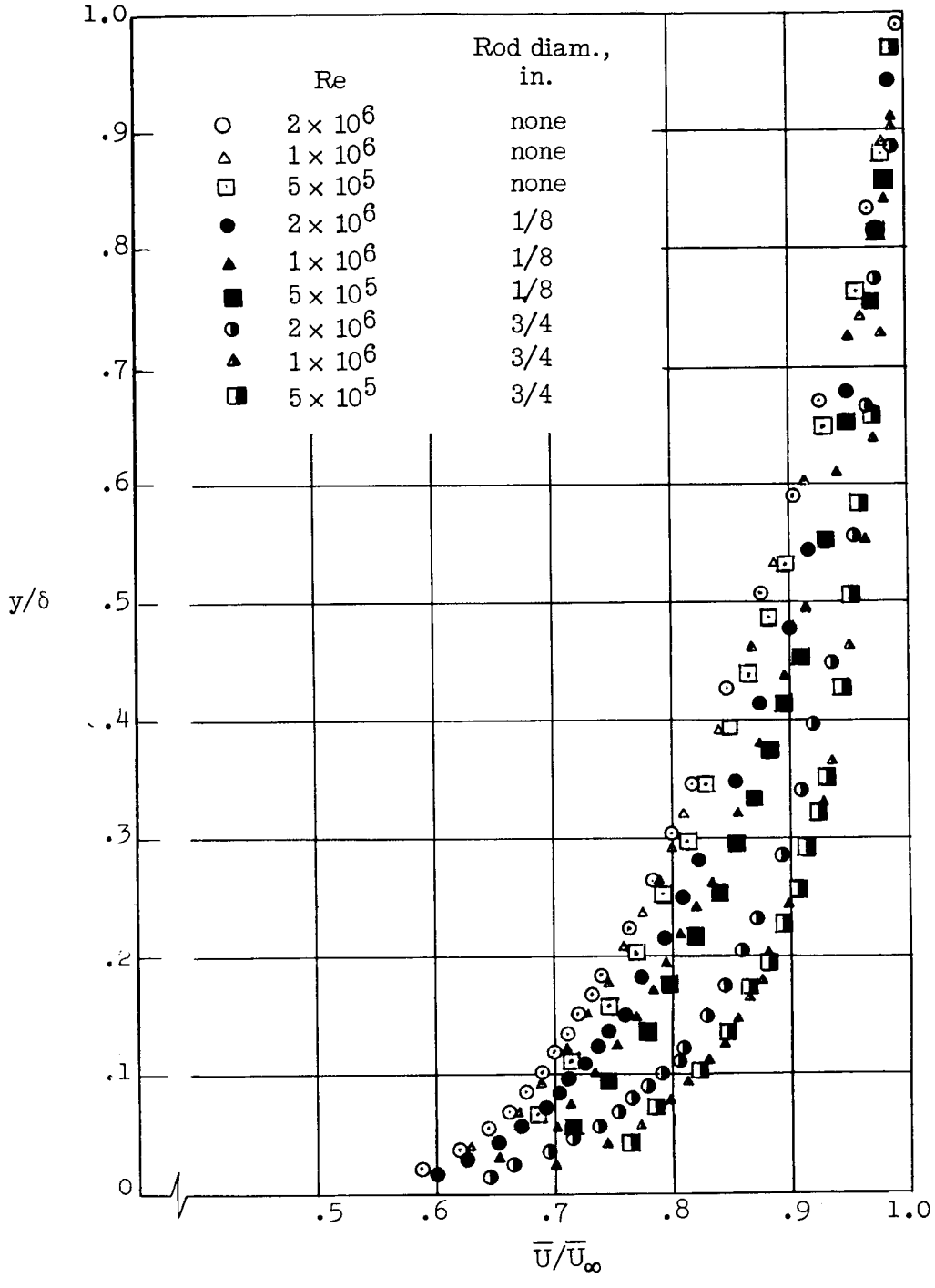

(b) Dimensionless profiles.

Figure 17.- Concluded.

W-136